Precambrian Research 366 (2021) 106422

Contents lists available at ScienceDirect

Precambrian Research

journal homepage: www.elsevier.com/locate/precamres

Geochronological constraints on the geological history and gold mineralization in the Tick Hill region, Mt Isa Inlier

Truong X. Le [a,b,*], Paul H.G.M. Dirks [a], Ioan V. Sanislav [a], Jan M. Huizenga [a,c,d], Helen A. Cocker [a], Grace N. Manestar [a]

[a] EGRU (Economic Geology Research Centre), College of Science and Engineering, James Cook University, Townsville, Queensland 4811, Australia
[b] Faculty of Geosciences and Geology Engineering, Hanoi University of Mining and Geology, 18 Pho Vien, Duc Thang, Bac Tu Liem Hanoi, Vietnam
[c] Department of Geology, University of Johannesburg, PO Box 524, Auckland Park 2006, Johannesburg, South Africa
[d] Faculty of Environmental Sciences and Natural Resource Management, Norwegian University of Life Sciences, Postbox 5003, NO-1432, Ås, Norway

ARTICLE INFO

Keywords:
Mt Isa
Mary Kathleen
Tick Hill
Gold deposit
U-Pb zircon

ABSTRACT

The Tick Hill Gold deposit in the southern Mary Kathleen Domain of the Mount Isa Inlier is hosted in a strongly deformed, Paleoproterozoic volcano-sedimentary sequence intruded by pre- and syn-tectonic granites. Igneous rocks and quartzite from the Tick Hill region were dated to constrain the age of the lithologies, deformation events, and gold mineralization. LA-ICP-MS, U-Pb zircon ages for these rocks, together with field relationships, confirm the presence of: (1) 1855–1850 granite belonging to the Kalkadoon Supersuite at ~10 km and ~4 km west of Tick Hill, respectively; (2) 1790–1770 Ma early syn-tectonic granite along the contact zone between mapped Argylla Formation and the Kalkadoon Supersuite west of Tick Hill, and later syn-tectonic leucogranite within the immediate vicinity of Tick Hill, including the host rocks to gold mineralization; and (3) late-tectonic, 1525–1520 Ma pegmatite and associated hydrothermal activity in the Tick Hill area that resulted in the mobilization of gold. Quartzite ridges in the hanging wall and footwall of the orebody provided contrasting results, with the youngest zircon population groupings at ca. 1781 Ma and 1841 Ma, respectively. Textural evidence suggests that much of the hanging wall quartzite is probably metasomatic in origin, and the ca. 1781 Ma age group, which was derived from mostly prismatic, euhedral zircon, reflects the age of a heavily silicified quartzofeldspathic gneiss. Thus, the age of the youngest detrital zircon group, ca. 1841 Ma, constrains the maximum age of the sequence at Tick Hill. Field evidence suggests that the 1790–1770 Ma granites intruded into the sedimentary sequence that hosts gold mineralization, indicating that the supracrustal rocks are at least ca. 1790 Ma in age and should not be grouped as Corella Formation. These sediments were affected by intense shearing and upright folding between 1790 Ma and 1770 Ma and younger normal faulting and metasomatism around 1525–1520 Ma. Early gold was introduced during D_1 peak metamorphism at 1790–1770 Ma while the later mineralizing events involved the new introduction of gold or the remobilization of pre-existing older gold around 1525–1520 Ma. One of the major outcomes of this study is that the old schist zones in the south Mary Kathleen Domain are prospective for gold mineralization.

1. Introduction

The Mount Isa Inlier is a highly mineralised geological terrain with world-class deposits of lead, zinc, and copper (Withnall and Hutton, 2013). Most major Pb-Zn deposits are concentrated in 1570–1660 Ma shale units in the western part of the inlier (Huston et al., 2006; Denaro et al., 2013). The bulk of IOCG mineralization is concentrated in the eastern part of the inlier where mineralization occurs in supracrustal rocks that are spatially associated with intrusions of the 1550–1490 Ma Williams and Naraku Suites (Page and Sun, 1998; Perkins and Wyborn, 1998; Williams et al., 2005, Neumann and Fraser, 2007). In the central part of the Mt Isa Inlier, which includes the higher-grade gneisses of the Kalkadoon-Leichhardt Belt and adjacent rocks of the Mary Kathleen Domain (MKD), mineralization appears to be less abundant. Mineral deposits in the MKD include the world-class Dugald River Pb-Zn-Ag deposit, many smaller Cu-Au occurrences (e.g., Elaine Dorothy,

* Corresponding author at: EGRU (Economic Geology Research Centre), College of Science and Engineering, James Cook University, Townsville, Queensland 4811, Australia.
E-mail address: truong.le@my.jcu.edu.au (T.X. Le).

https://doi.org/10.1016/j.precamres.2021.106422
Received 17 November 2020; Received in revised form 31 August 2021; Accepted 1 October 2021
Available online 11 October 2021
0301-9268/© 2021 Elsevier B.V. All rights reserved.

Trekelano, Mount Colin, Overlander, Kalman), the Mary Kathleen U-REE deposit (Forrestal et al., 1998; Denaro et al., 2013), and the gold-only, high-grade Tick Hill deposit, which is the focus of this study. The Tick Hill deposit is a relatively small, but an extremely rich, gold-only deposit, and constitutes a unique mineralization style in the Mt Isa Inlier. The timing of mineralization and links to other, IOCG-related gold deposits in the Mt Isa Inlier have not been established, and the deposit is variably referred to as either an end-member IOCG deposit (e.g., Williams et al., 2005; Groves et al., 2010), or an orogenic, shear zone-hosted deposit (e.g., Denaro et al., 2013).

Compared to other parts of the Mt Isa Province, relatively little geochronological and stratigraphic work has been completed in the MKD. The current interpretation of stratigraphy and structural evolution of the MKD, including associated mineralization, is largely based on work performed in the central MKD (e.g., Blake et al. 1984; Holcombe et al., 1991; Neumann et al., 2006; Neumann et al., 2009; Southgate et al. 2013; Withnall and Hutton, 2013). Far fewer geochronological constraints are available for rocks in the northern and southern parts of the MKD (e.g., Kositcin et al, 2019; Withnall, 2019; Bodorkos et al., 2020). Rocks in the MKD have been mainly attributed to 1780–1730 volcano-sedimentary sequences (e.g., Oliver et al., 1991; Foster and Austin, 2008; Neumann et al., 2009; Withnall and Hutton, 2013; Kositcin et al, 2019), with deformation attributed to 1755–1740 Ma extensional and 1600–1500 Ma compressional events (e.g., Holcombe et al., 1991; Blake and Steward, 1992; Withnall and Hutton, 2013). The MKD is characterized by abundant 1740–1730 Ma intrusions of the Wonga and Burstall Suites. Intrusions of the younger Williams Suite are conspicuously absent (e.g., Kositcin et al, 2019; Withnall, 2019; Bodorkos et al., 2020; Spence et al., 2021). In the absence of good age constraints in the southern MKD, the volcano-sedimentary sequences in the Tick Hill area have generally been correlated with the Argylla and Corella Formations further north (e.g., Blake et al., 1982; Wyborn, 1997; Withnall and Hutton, 2013; Withnall, 2019), whilst upright folding of high-grade gneiss around Tick Hill was linked to east–west compression during the Isan Orogeny by analogy with similar folding in the Mary Kathleen and Duchess areas (e.g., Holcombe et al., 1991, Oliver et al., 1991; Passchier, 1992; Choy, 1994). Blake (1980) and Blake et al. (1982) pointed out that care should be taken when making regional correlations, i.e. the high-grade Corella Formation west of the Wonga belt including gneisses in the Tick Hill area could actually represent pre-1860 Ma basement. The age of mineralization at Tick Hill remains unconstrained and has variably been linked to ca. 1740 Ma extensional events and associated magmatism (Choy, 1994; Forrestal et al., 1998), or undefined younger (ca. 1530 Ma) intrusive activity (e.g., Rutherford, 1999; Tedman-Jones, 2001), with little direct evidence provided in support.

In this paper, we present new U-Pb zircon ages and whole-rock geochemistry for a range of igneous and quartzitic units with variable relationships to the dominant gneissic fabrics in the Tick Hill area (i.e., pre-, syn- and post $D_{1\text{-}2}$). Samples were obtained from exploration drill core and from outcrops within a 10 km radius of the Tick Hill open pit (Fig. 3). In dating the selected rocks we aim to constrain: (1) the age of igneous events in the area; (2) the extent of Kalkadoon-Leichhardt Belt basement gneiss; (3) the age of the main stratigraphic units that host the Tick Hill deposit; (4) the timing of deformation events that affected the deposit; and (5) the timing of mineralization.

2. Geological setting

2.1. Regional geology

The Mt Isa Inlier preserves a complex mixture of bimodal igneous rocks and Paleo- to Meso-Proterozoic tectono-stratigraphic sequences that formed during a 400-million year period (1890–1500 Ma) in a series of discontinuous basins. These basinal sequences were affected by magmatism and metamorphism related to two major orogenic events, the Barramundi Orogeny (1870–1840 Ma) and the Isan Orogeny (1600–1500 Ma; Blake and Steward, 1992; Abu Sharib and Sanislav, 2013; Withnall and Hutton, 2013). Based on the distribution and age of sedimentary sequences and intrusive igneous suites, the Mt Isa Province was subdivided into three north-trending tectonic domains (Blake, 1987; Withnall and Hutton, 2013): the Western Fold Belt; the Kalkadoon-Leichhardt Belt; and the Eastern Fold Belt (Fig. 1). The Kalkadoon-Leichhardt Belt, represents an old (>1850 Ma) basement that exposes rocks affected by the Barramundi Orogeny. It is overlain by younger rocks to the west and east. Post-Barramundi, volcano-sedimentary cover sequences in the inlier have been interpreted as intracratonic rift-sag deposits (e.g., Blake and Steward, 1992; Foster and Austin, 2008; Withnall and Hutton, 2013) and were described as three separate cover sequences separated by regional unconformities. The age and extent of the cover sequences were later refined with additional geochronological and stratigraphic work and the sequences were subsequently linked to the development of three 'superbasins' (Jackson et al., 2000; Scott et al., 2000; Neumann and Fraser, 2007; Foster and Austin, 2008; Neumann et al., 2009; Withnall and Hutton, 2013; Fig. 2). Following the stratigraphic subdivisions as outlined in Foster and Austin (2008), the cover sediments include Cover Sequence 1 (1890–1850 Ma), which predated the development of the superbasins, is largely composed of felsic volcanics, and is restricted to the Kalkadoon-Leichhardt Belt and Western Fold Belt (Fig. 2). This is overlain by Cover Sequence 2 (1790–1690), which overlaps with the Leichardt (1800–1750 Ma) and Calvert (1730–1690 Ma) Superbasins and includes felsic volcanics of the Argylla Formation and calc-silicates of the Corella Formation that are prominent in the MKD (Fig. 2). This Cover Sequence 2 is overlain by Cover Sequence 3 (1680–1590 Ma), which overlaps with the Isa Superbasin (1665–1575 Ma) and is distributed widely across the entire Mt Isa Province (Fig. 2). Development of the various superbasins was accompanied by igneous activity, which involved extensive volcanism and the emplacement of bimodal igneous batholiths along north-trending belts. These include emplacement of the 1860–1850 Ma Kalkadoon Supersuite into basement gneiss of the Kalkadoon-Leichhardt

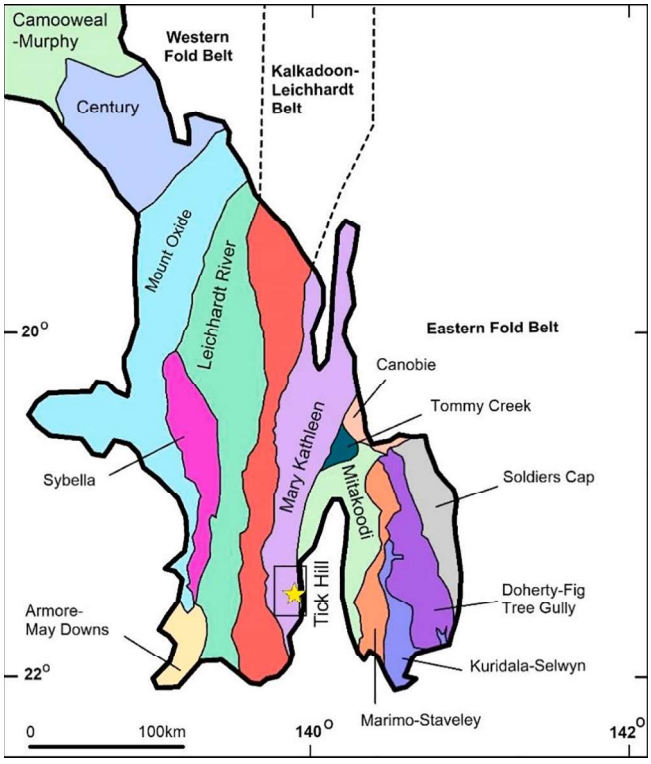


Fig. 1. Tectonic subdivisions in the Mt Isa Inlier (adapted from Blake, 1987; Withnall and Hutton, 2013). The black box shows the area shown in Fig. 3a.

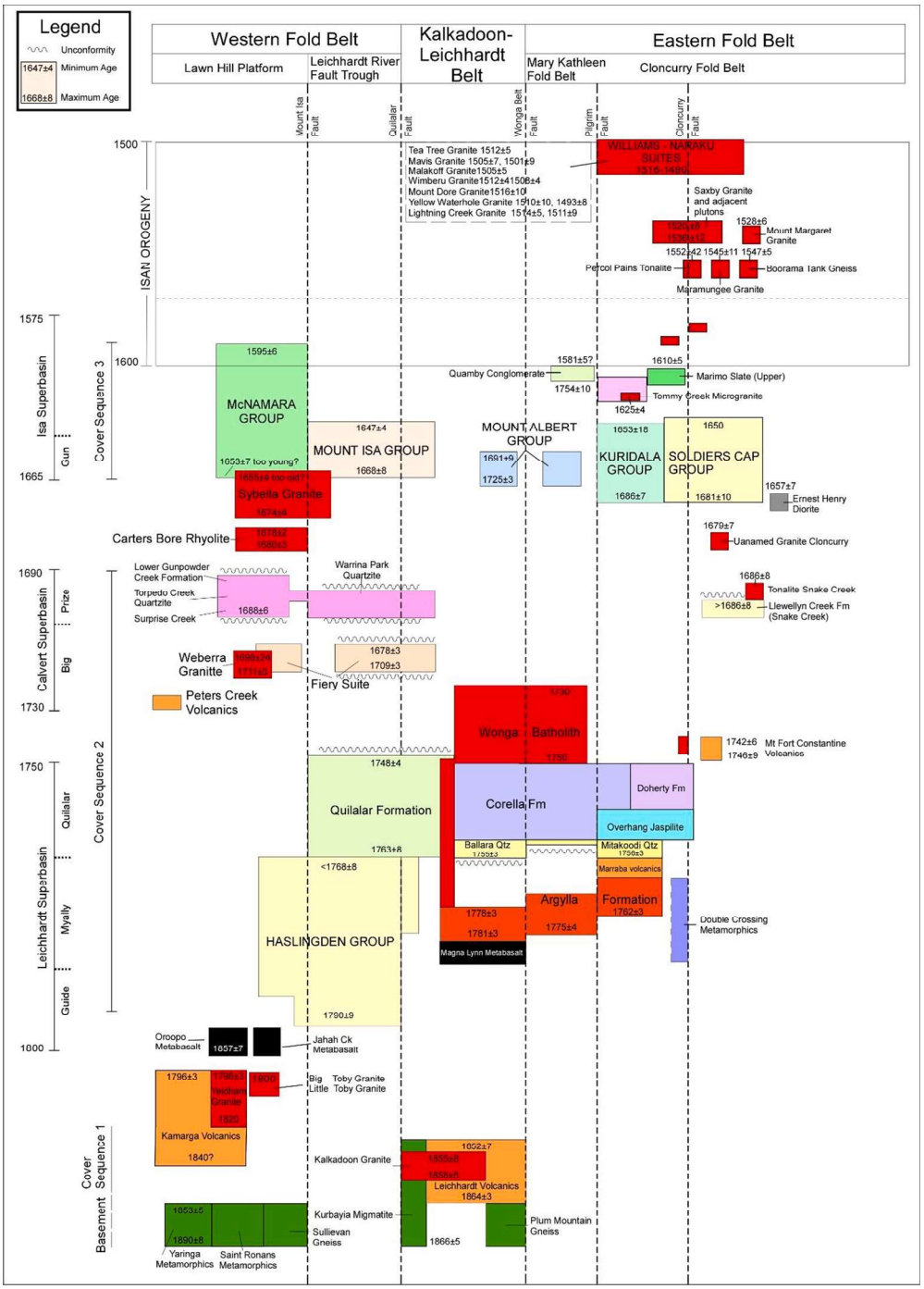


Fig. 2. Chronostratigraphic time–space plot for the Mt Isa Inlier (after Foster and Austin, 2008; Withall and Hutton, 2013).

Belt; the 1780–1720 Ma Wonga and Burstall Suites along the western margin of the Eastern Fold Belt and the 1675–1655 Ma Sybella Suite along the western margin of the Western Fold Belt. In addition, post-tectonic suites of the 1550–1490 Ma, Williams and Naraku Suites were emplaced across much of the Eastern Fold Belt, during the final stages of the Isan Orogeny (Page and Sun, 1998; Withnall and Hutton, 2013).

Rocks in the Eastern Fold Belt were further subdivided into a series of mostly north-trending, unconformity and fault-bounded tectono-stratigraphic domains, the westernmost of which is the MKD (e.g., Withnall and Hutton, 2013). The MKD is bounded by the Pilgrim-Rose Bee Fault Zone to the east and comprises 1780–1730 Ma volcano-sedimentary rocks belonging to Cover Sequence 2 (Upper Leichardt Superbasin), which in the northern part of the domain are overlain by rocks of the Mount Albert Group of Cover Sequence 3 (i.e., Isa Superbasin; e.g., Scott et al., 2000; Foster and Austin, 2008; Fig. 2). To the west of the MKD, rocks of Cover Sequence 2 overly the Kalkadoon-Leichhardt basement and are intruded by granites and gabbros of the Wonga and Burstall Suites (Withnall and Hutton, 2013; Kositcin et al., 2019; Bodorkos et al., 2020; Spence et al., 2021).

The stratigraphic base of Cover Sequence 2 in the Kalkadoon-Leichhardt Belt consists of the ca. 1790 Ma Magna Lynn Metabasalt unit (Blake, 1987; Jackson et al., 2000; Foster and Austin, 2008; Carson et al., 2011; Withnall and Hutton, 2013), which is overlain by felsic volcanics of the 1770–1780 Ma Argylla Formation (Page, 1983; Neumann et al., 2009) that extend into the MKD (Fig. 2). The Argylla Formation is overlain by the ca.1755 Ma Ballara Quartzite (Blake, 1987;

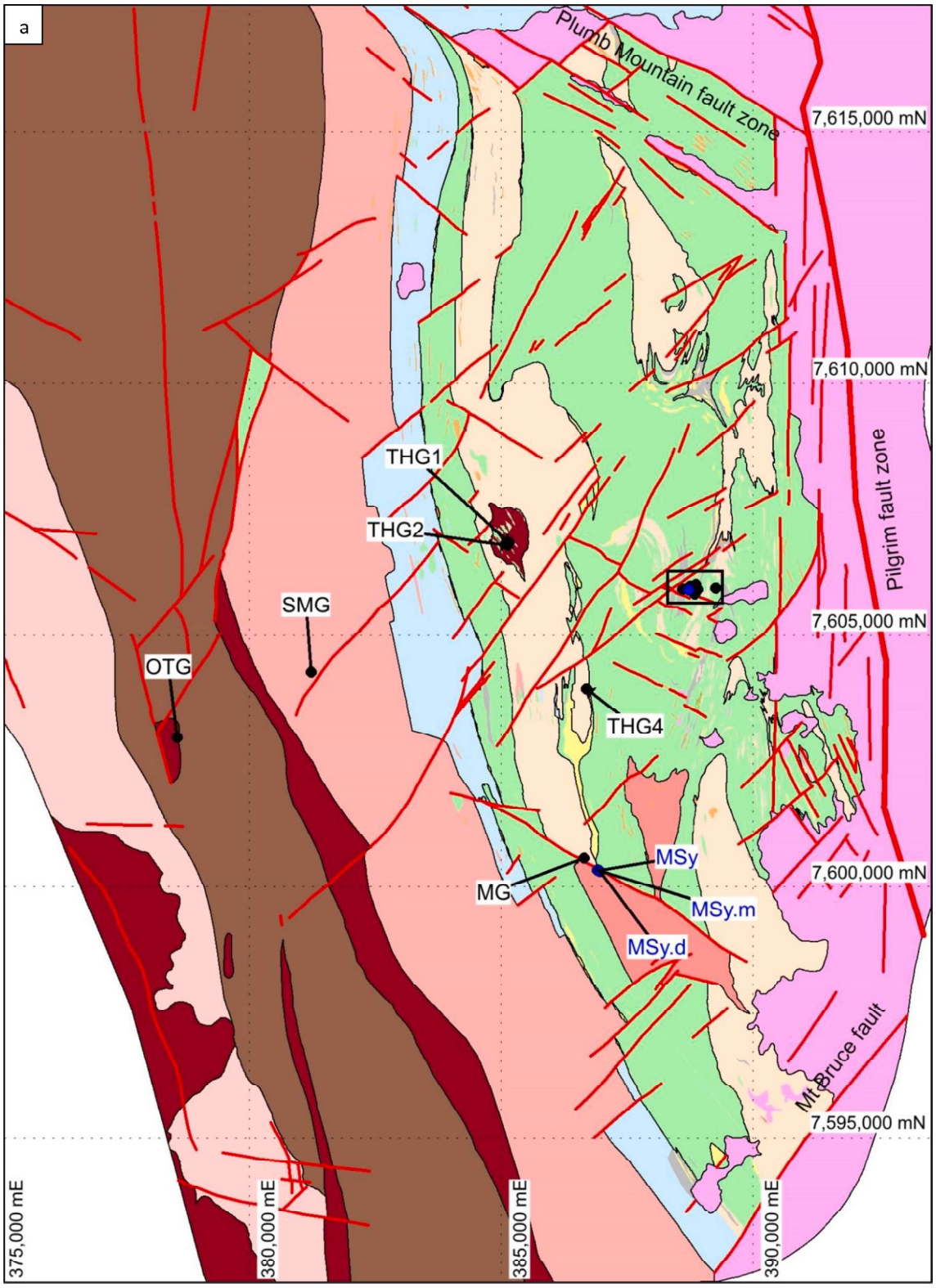


Fig. 3. Geological map of the Tick Hill region (a; after Blake et al., 1982; Wyborn, 1997; Rutherford 2000) with the locations of geochronological (black lettering) and geochemical samples (blue lettering). The black box shows (b) the close-up of the pit area. The location of drill core collars from which samples TH66, TH86, TH108 and TH140 were taken, are shown.

Neumann et al., 2006; Neumann et al., 2009) and the 1730–1760 Ma Corella Formation that covers large parts of the MKD (Blake, 1980; Blake, 1987; Carson et al., 2009; Southgate et al., 2013; Withnall and Hutton, 2013). At the type locality northeast of Mary Kathleen, the Corella Formation consists of scapolite-bearing calc-silicate and amphibolite, with lesser marble, metapelite, quartzite, and felsic meta-volcanics (Blake, 1987; Foster and Austin, 2008). The calc-silicates have been interpreted as metamorphosed, shallow water, mixed siliciclastic-

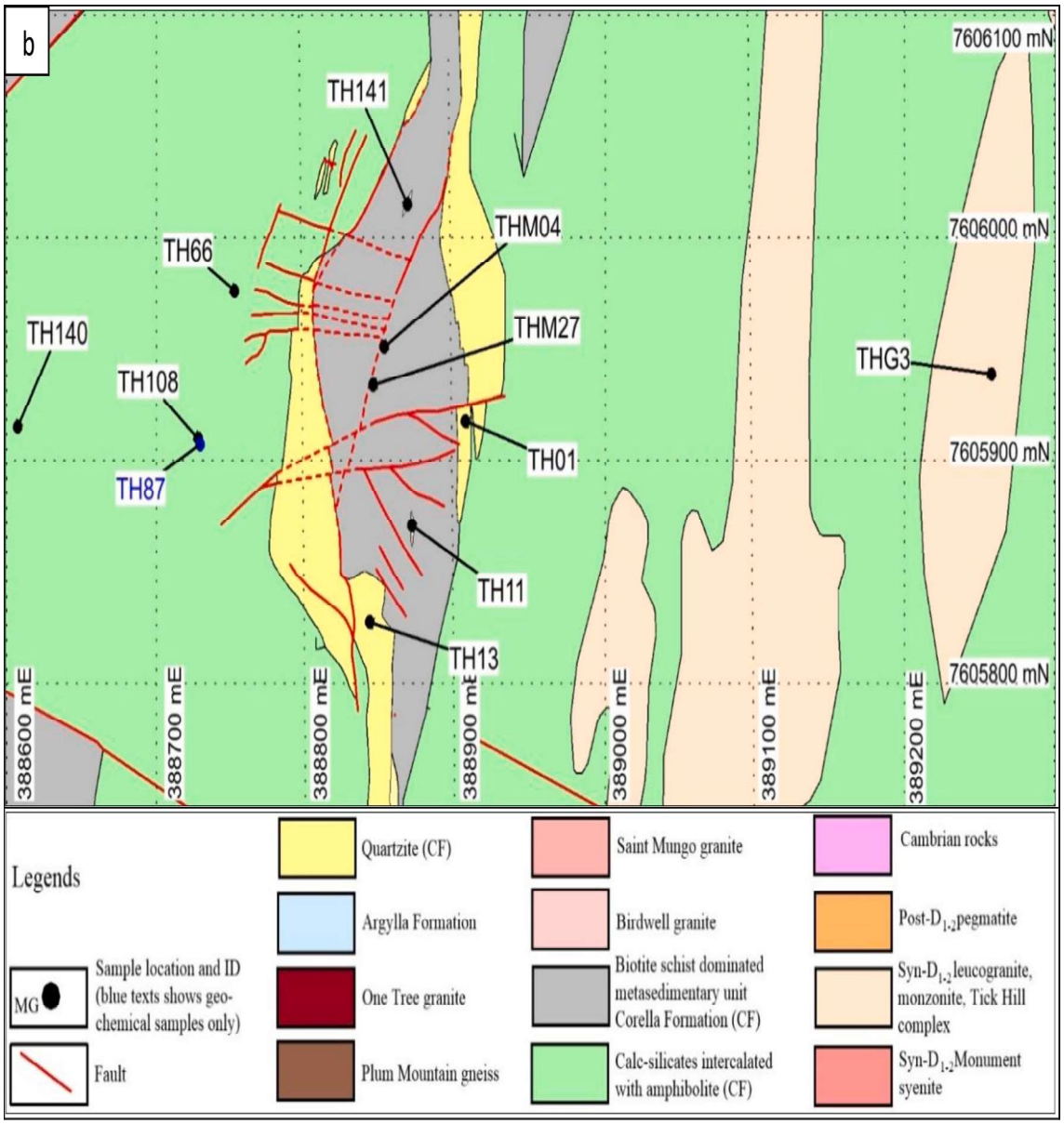


Fig. 3. (*continued*).

carbonate platform sequences intercalated with evaporite deposits (e.g., Blake, 1987; Jackson et al., 2000; Foster and Austin, 2008).

In the Tick Hill region (Fig. 3a), rocks are dominated by calc-silicate and amphibolite, intercalated with quartzite and biotite-schist, which have been correlated with the Corella Formation to the north (Blake et al., 1982; Wyborn, 1997). However, it has been suggested that the metasediments around Tick Hill could represent pre-1860 Ma basement (Blake, 1980). Much of the quartzite in the area occurs along discontinuous ridges. Exploration reports mention that these quartzite ridges are characterized by early brecciation and veining, have diffuse boundaries and commonly transect the gneissic layering. Consequently, they were interpreted as early metasomatic alteration zones along shears, rather than sedimentary units (e.g., Laing, 1993; Oliver, 1995). Felsic metavolcanics, which outcrop along a north-trending zone to the west of the calc-silicates (Fig. 3a) were assigned to the Argylla Formation (Blake et al., 1982; Wyborn, 1997). West of the Argylla Formation are a series of north-trending gneissic granites, which mark the transition into Kalkadoon-Leichhardt basement rocks (Fig. 3a; Withnall and Hutton, 2013). From east to west, these are the Saint Mungo Granite, the One Tree Granite, the Plum Mountain Gneiss and the Birds Well Granite (Fig. 3a; Blake et al., 1982; Wyborn, 1997), which were targeted for geochronology in this study. The metasedimentary units around Tick Hill were intruded by syn-tectonic granite sheets of the Tick Hill Complex, and the syn-tectonic Monument Syenite (Laing, 1993; Wyborn, 1997; Rutherford, 1999; Rutherford, 2000). A small inlier of Saint Mungo Granite was locally mapped within intrusions of the Tick Hill Complex immediately west of Tick Hill (Rutherford, 1999; Rutherford, 2000). In the light of new geochronological data from this study, the rock is corrected as remnant Kalkadoon Supersuite (i.e., One Tree Granite; Fig. 3a). Together with the Saint Mungo and Birds Well Granites, the intrusions of the Tick Hill Complex were assigned to the ca. 1740 Ma Wonga and Burstall Suites (Wyborn, 1997; Rutherford, 1999; Rutherford, 2000). Post-tectonic (post-D_1) intrusions are limited to small outcrops of pegmatite and aplitic granite originally described as granite of unknown age (Blake et al., 1982, Wyborn, 1997) and later assigned to the Williams Suite (Laing, 1993; Rutherford, 2000).

The gneisses around the Tick Hill deposit record four major deformational events (e.g., Blake et al., 1982; Passchier and Williams, 1989; Oliver, 1995; Tedman-Jones, 2001; Le et al., 2021). D_1 events involved the formation of an upper amphibolite facies mylonitic S_1 fabric

associated with isoclinal intrafolial folds, a west-dipping lineation, and a possible east-up sense of movement. D_1 structures were interpreted to result from north-south extension around 1750–1730 Ma equivalent to what has been described for the Wonga-Shinfield zone further north (e.g., Passchier and Williams, 1989; Holcombe et al., 1991; Passchier, 1992; Oliver, 1995; Withnall and Hutton, 2013). During D_2, the S_1 mylonite fabric was folded to form a north-trending steeply dipping high-strain zone and associated tight upright folds that characterize the Tick Hill area (Laing, 1993; MacCready et al., 1998). The D_2 event resulted from east-west compression at high-grade metamorphic conditions during the Isan Orogeny (Oliver, 1995; Betts et al., 2006), based on correlations with structures in the Mary Kathleen and Duchess areas (e.g., Holcombe et al., 1991; Passchier, 1992). During $D_{1\text{-}2}$, rocks in the MKD were affected by high-temperature, low-pressure metamorphism (550–670 °C, 3–4 kbar in the Mary Kathleen area), accompanied by the emplacement of the Wonga and Burstall granites (Oliver et al., 1991). Mineralization and related alteration generally overprinted the $S_{1\text{-}2}$ fabrics, although gold has been described from inclusions in peak-metamorphic assemblages leading to suggestions that some of the mineralization may have had an early origin (e.g., Choy, 1994; Oliver, 1995; Tedman-Jones, 2001; Le et al., 2021Le et al., 2021).

D_3 events in the Tick Hill pit are characterized by the formation of brittle-ductile normal faults and breccia formation. Gold mineralization, and associated chlorite-albite-hematite-quartz alteration occurred at this time, probably concomitant with the emplacement of late-tectonic pegmatite (Le et al., 2021). The regional extent of the D_3 events has not been established.

D_4 events involved the formation of northeast-striking dextral and northwest-striking sinistral faults including the Plum Mountain and Mt Bruce Faults (Fig. 3a) to the north and south of Tick Hill, respectively. D_4 faults post-dated Tick Hill mineralization (Le et al., 2021) and resulted in cataclasite formation and clay alteration. Regionally, these faults have been linked to east–west compression during the late stages of the Isan Orogeny (O'dea et al., 1997; Forrestal et al., 1998; Betts et al., 2006) coeval with the emplacement of the Williams Suite and widespread sodic-potassic and hematite-rich alteration (Wyborn et al., 1988). Brittle reactivation of these faults occurred at various stages during later events between 1500 Ma and 1100 Ma (e.g., Blake and Steward, 1992; Oliver, 1995).

2.2. Previous geochronology in the Mary Kathleen Domain

Past geochronological studies conducted in the MKD defined three main magmatic events: (1) emplacement of the Leichhardt Volcanics and Kalkadoon Supersuite at 1865–1845 Ma (Page 1978; Carson et al., 2011; Kositcin et al., 2019); (2) bi-modal volcanism resulting in deposition of the Magna Lynn Metabasalt and Argylla Formation on top of Kalkadoon-Leichhardt basement at 1800–1775 Ma with associated magmatism during a possible early extensional event (Page, 1978; Page and Sun, 1998; Carson et al., 2009; Neumann et al., 2009; Carson et al., 2011; Magee et al., 2012; Kositcin et al., 2019); and (3) emplacement of granites belonging to the Wonga and Burstall Suites at 1745–1730 Ma (Page, 1978; Page, 1983; Pearson et al., 1992; Page and Sun, 1998; Davis et al., 2001; Carson et al., 2009; Neumann et al., 2009; Geoscience Australia, 2011; Kositcin et al., 2019), during further extension (e.g., Holcombe et al., 1991; Withnall and Hutton, 2013). The summary of geochronological study results in the MKD is presented in Appendix 1.

The host rocks of the Tick Hill deposit were mapped as Corella Formation (Blake et al., 1982; Rutherford, 2000), which was dated at 1755–1740 Ma using detrital zircons, intercalated volcanic horizons and intrusions from samples collected further north (Table 2; Page and Sun 1998; Carson et al., 2009; Neumann et al., 2009; Geoscience Australia, 2011; Kositcin et al., 2019). Metamorphic ages in the MKD obtained from titanite or the overgrowths on primary zircon grains are mainly at 1515–1500 Ma (Table 2; Kositcin et al., 2019).

Little age dating has been done in the immediate vicinity of the Tick Hill mine. An imprecise K-Ar biotite age of ca.1420 Ma (Richards et al., 1963) was reported for the Monument Syenite, 4 km south of Tick Hill, whilst a sample of Plum Mountain Gneiss in the Kalkadoon-Leichhardt basement 20 km northwest of Tick Hill yielded a U-Pb zircon age of 1862 ± 3 Ma (Carson et al., 2011). Poorly constrained titanite ages mentioned in consulting reports (Tedman-Jones, 2001) include a 1517 ± 10 Ma titanite age interpreted to predate mineralization, and a 1433 ± 85 Ma titanite age interpreted to postdate mineralization. In addition, lead isotopic data for pyrite associated with gold mineralization yielded an isochron age of 1530 ± 100 Ma (Tedman-Jones, 2001).

3. Sample descriptions

Sixteen samples from rock units in the immediate vicinity of the Tick Hill deposit (10 samples) and surrounding areas (six samples, Fig. 3) were collected for dating. In collecting the samples, reference was made to unit names of the 1:100,000 scale geological maps compiled by Blake et al. (1982), Wyborn (1997) and later digital versions. Two regional samples (OTG and SMG) were taken from granitic gneiss to the west of the mapped western boundary of the Argylla Formation while four regional samples (THG1, THG2, THG4 and MG) were taken from intrusions to the east of the mapped outcrop of Argylla Formation. Local samples collected in and around the Tick Hill pit includes eight syn-$D_{1\text{-}2}$ to D_3 igneous units (samples THG3, THM04, THM27, TH11, TH66, TH106, TH140 and TH141) and two quartzite samples (TH01 and TH13). The 16 samples were taken to constrain the age of pre-D_1 and syn-$D_{1\text{-}3}$ deformation events and the host sequence at the Tick Hill region. In addition, four samples from post-tectonic pegmatite and Monument Syenite that did not yield (sufficient) zircon grains were used for major and trace element geochemistry to further characterize the igneous suites in the Tick Hill area. The summary of samples is shown in Table 3 whilst their details are described as following.

3.1. Regional samples

Sample OTG is a granitic gneiss that was collected from the One Tree Granite, which is part of the Kalkadoon Supersuite, intruded the ca. 1860 Ma Plum Mountain Gneiss, 10 km west of the Tick Hill pit (Fig. 3a; Blake et al., 1982; Carson et al., 2011). The granite preserves a well-developed, north-trending foliation (Fig. 4a) with a steeply plunging lineation defined by aligned biotite, amphibole and elongated quartz-feldspar aggregates. The sample is composed of ~30% quartz and ~50% feldspar (plagioclase and K-feldspar), ~15% amphibole and biotite, and ~5% magnetite. In places, plagioclase was altered to sericite while biotite was replaced by chlorite.

Sample SMG was collected from outcrops of granitic gneiss mapped as Saint Mungo Granite (Blake et al., 1982; Rutherford, 2000) along the main farm track, ~8 km west of the Tick Hill pit (Fig. 3a) which was interpreted to have intruded the Corella Formation (Blake et al., 1982). The SMG intruded Plum Mountain Gneiss and the Corella Formation, with outcrops of Corella schist occurring west of the intrusion in conformable contact with Plum Mountain Gneiss (Blake et al., 1982). The rock preserves a foliation (Fig. 4b) defined by biotite, that wraps around partly recrystallized, cm-large feldspar grains. It is composed of ~35% quartz and ~40% feldspar (K-feldspar and plagioclase), ~20% amphibole and biotite and ~5% magnetite. Alteration of plagioclase to sericite and silicification of amphibole was common.

Samples THG1 and THG2 are two phases of granitic gneiss variably mapped as Tick Hill Granite or Saint Mungo Granite. These samples were collected from low outcrops along a farm road, ~4 km west of the pit (Fig. 3a), which contain rafts of Corella Formation (Blake et al., 1982; Wyborn, 1997). Sample THG1 was collected from a northwest-trending 5–10 m wide granitic dyke that intruded older granitic gneiss that was sampled as THG2 (Fig. 4c). Both phases of granite are strongly foliated, and the dyke from which THG1 was taken truncates the foliation in the older granite at a low angle (<10°). Sample THG1 consists of well-

Table 1
Major (wt%) and trace (ppm, except for Au which is in ppb) element contents for samples from the Tick Hill region. Samples TH87 and TH108 were not analysed for trace elements and FeO.

Spl./oxi./ele.	OTG	THG2	SMG	THG1	MG	THG4	THG3	THM04	THM27	TH141	TH11	TH140	TH66	TH108	TH87	Msy	Msy.m	Msy.d
SiO2	69.32	68.13	70.40	70.36	60.90	74.56	75.12	80.63	76.21	64.06	61.42	67.19	76.23	59.26	64.81	51.76	52.49	49.79
Al2O3	13.01	14.51	13.81	13.54	21.30	14.93	14.71	10.52	13.04	20.9	20.36	18.57	13.14	22.46	19.76	20.64	22.43	23.17
Fe2O3	6.21	3.60	4.18	3.74	1.56	0.12	0.09	1.68	1.75	1.27	2.70	1.14	0.89	0.23	0.49	8.15	5.11	5.66
FeO	5.78	3.28	3.61	2.96	0.67	0.36	0.35	1.07	0.95	0.44	2.19	1.09	0.6	–	–	5.04	3.07	3.78
MgO	1.18	1.00	0.41	0.84	0.88	0.19	0.20	0.47	0.65	0.7	1.42	1.19	0.29	1.31	0.78	1.45	0.78	1.03
CaO	2.30	2.34	1.82	2.39	3.55	1.35	1.41	0.44	0.66	0.76	2.68	2.62	1.06	3.08	2.53	3.97	2.45	3.19
Na2O	1.66	2.27	1.56	2.96	5.63	6.33	5.94	5.13	5.53	6.2	4.04	5.81	1.29	6.54	5.40	8.34	10.87	9.73
K2O	3.30	4.49	5.73	5.14	1.44	0.94	0.80	0.54	1.03	4.26	3.04	1.81	6.89	2.05	1.63	3.14	3.40	3.37
TiO2	0.75	0.54	0.40	0.59	0.44	0.03	0.03	0.02	0.13	0.03	0.47	0.21	0.08	0.65	0.07	0.77	0.51	0.56
P2O5	0.21	0.25	0.15	0.21	0.07	0.15	0.13	0.01	<0.01	<0.01	0.07	0.01	0.08	0.07	0.10	0.36	0.25	0.35
MnO	0.07	0.02	0.04	0.03	0.02	0.01	0.01	0.02	0.02	0.02	0.02	0.02	0.01	0.03	0.03	0.16	0.10	0.11
LOI	0.43	0.63	0.45	0.53	1.55	0.51	0.62	0.5	0.9	1.6	1.85	1.3	0.50	2.91	1.81	0.80	0.40	0.77
Sum	98.46	97.80	98.96	100.37	97.40	99.15	99.10	99.98	99.97	99.86	98.11	99.9	100.48	98.62	97.44	99.69	98.95	97.93
Ba	920	706	699	817	808	110	118	36	111	371	307	197	147	–	–	1232	1656	1737
Cs	9.9	4.1	9.7	2.1	3.9	<0.1	0.2	<0.1	1.2	0.6	3.1	1.4	0.7	–	–	1.5	0.5	1.1
Ga	16.6	20.1	18.8	18.1	12.5	11.9	12.2	10.6	13.9	17.5	20.6	18.1	18.8	–	–	16.8	15.6	15.4
Hf	8.3	3.9	9	8.7	6.7	1.5	2.2	0.2	1.2	10.9	3.4	7.2	2.9	–	–	2.3	1.3	1.4
Nb	14.2	15.1	13.2	19.4	6.2	2	0.8	1.6	3.7	0.4	4.7	2.7	4.2	–	–	26.5	16.7	16.5
Rb	126.9	192.8	229.4	165.4	176.6	17.4	11.5	10.3	34	223.8	159.1	66.4	109.1	–	–	72.8	63.7	61.9
Sn	6	<1	7	1	<1	<1	<1	<1	<1	<1	<1	<1	<1	–	–	<1	<1	<1
Sr	130.2	140.3	79	128.5	98	135.4	154.7	25.3	79.1	230.8	230.6	240.1	297.4	–	–	576.1	614.1	711.6
Ta	1	1.6	1.3	1.7	1.3	0.3	0.1	<0.1	0.2	<0.1	0.6	1.3	0.5	–	–	1.2	0.7	0.8
Th	18.7	10.8	31.4	31.3	130.7	3.3	2.9	0.5	2.8	5.4	3.1	2.9	0.5	–	–	1.4	1	0.7
U	2.3	7.7	5.8	7.4	35.7	0.6	0.5	0.4	2.7	1.7	1	1.5	0.7	–	–	0.3	0.2	0.1
V	41	40	13	23	<8	<8	<8	<8	16	9	61	34	<8	–	–	49	28	34
W	1.6	10.7	5	0.7	<0.5	0.5	1	<0.5	<0.5	<0.5	1.4	1	1.4	–	–	<0.5	0.7	<0.5
Zr	318.2	144.2	322	322.1	187.7	36.7	49.4	9.1	49.1	428.5	120.1	215.7	100.1	–	–	80.5	46.1	48.2
Y	26.9	22.2	52.1	54.7	9	4.2	3	0.8	3	7.1	4	4.1	0.9	–	–	16.3	9.8	13.2
La	82.3	26.5	86.2	76.3	70.5	1.3	2.8	1	4.6	16	5.9	5.4	4.1	–	–	18.7	12.2	16.6

Table 2
Historically geochronological data constraining the age of Corella Formation and metamorphic overprint in the Marry Kathleen Domain. The sample order from 1 to 9 is consistent with its locations from north to south of the domain.

#	Spl. ID	Zone 54-GDA94		Rock Name	Rock Type	Age (Ma)	Comments	Reference
		E	N					
1	92,208,025	414,632	7,754,495	Corella Fm.	Rhyolite	1750 ± 7	Felsic volcanics at Mt Roseby SSE of Dugald River.	Page and Sun (1998)
2	2,005,169,003	390,651	7,721,920	Corella Fm.	Quartzite	1776 ± 3		Neumann et al. (2009)
3	2,005,169,008	379,509	7,712,059	Corella Fm.	Quartzite	1770 ± 6		Neumann et al. (2009)
4	BB5903	386,775	7,672,701	Corella Fm.	Metarhyolite	1740 ± 5	Meta-rhyolite in the Corella Formation ~40 km north of Duchess	Kositcin et al. (2019)
5	BB5906	386,955	7,673,667	Corella Fm.	Metarhyolite	1739 ± 5	Meta-rhyolite in the Corella Formation ~40 km north of Duchess	Kositcin et al. (2019)
6	96,208,082	383,628	7,660,920	Corella Fm.	Rhyolite	1738 ± 2	Meta-rhyolite exposed in the Corella Formation ~30 km north of Duchess	Geoscience Australia (2011)
7	96,208,083	383,878	7,660,900	Corella Fm.	Quartzite	1740 ± 20	Near Mt Morah mine in the Duchess area	Geoscience Australia (2011)
8	BB5922	384,767	7,638,085	Corella Fm.	Micaceous feldspathic quartzite	1752 ± 2	About 3 km east of Duchess	Kositcin et al. (2019)
9	BB5933	381,752	7,639,530	Mount Erle Igneous Complex	Granite	1735 ± 3	The Corella Formation near Duchess is intruded by granite of the Mount Erle Igneous Complex	Geoscience Australia (2011)
10	BB5906	386,955	7,673,667	Corella Fm.	Metarhyolite	1515 ± 13	Metamorphic age. Rhyolite in the Corella Formation north of Duchess	Kositcin et al. (2019)
11	28G3	423,400	7,749,500	Dipvale Granodiorite	Granodiorite	1505 ± 7	Metamorphic age. Mt Erle Igneous Complex near Duchess and Mt Philp Breccia ~40 km north of Duchess	Davis et al. (2001)
12	BB5944	390,843	7,675,787	Mount Philp Breccia	Albite-actinolite-titanite rock	1503 ± 7	Metamorphic age. Mt Erle Igneous Complex near Duchess and Mt Philp Breccia ~40 km north of Duchess	Kositcin et al. (2019)
13	BB5933	381,752	7,639,530	Mount Erle Igneous Complex	Granite	1500 ± 6	Metamorphic age. The Corella Formation near Duchess is intruded by granite of the Mount Erle Igneous Complex	Kositcin et al. (2019)

foliated granitic gneiss (Fig. 4d) composed of <5 cm large subhedral K-feldspar porphyroclasts in a matrix of quartz, plagioclase and biotite, with minor hornblende. The dispersed, large, rounded feldspar clasts form the most conspicuous aspect of this rock. They are wrapped in a foliation that is defined by biotite and hornblende. Epidote, chlorite and sericite alteration is common in this sample. Sample THG2 consists of a strongly foliated granitic gneiss that is slightly more mafic than THG1, in which <1 cm large K-feldspar porphyroclasts with dynamically recrystallized margins are aligned within in a matrix of strongly foliated, quartz biotite and hornblende (Fig. 4e). The gneisses (i.e. samples THG1 and THG2) were mapped as part of the Tick Hill Complex (Blake et al., 1982; Wyborn, 1997) or as a Saint Mungo Granite outcrop surrounded by Tick Hill Complex in a more detailed exploration project (Rutherford, 1999; Rutherford, 2000). The Tick Hill complex intrudes the Corella Formation, showing rafts of Corella contained within the gneiss (Wyborn, 1997). The rock consists of quartz, plagioclase, microcline, biotite and minor hornblende (<1%), with a foliation defined by biotite. Compared to sample THG1, alteration is stronger in sample THG2, with plagioclase replaced by sericite, and microcline and biotite weakly altered to sericite and chlorite, respectively. Near the sampling site, the THG2 gneiss unit contains numerous large (up to 10′s of meters) enclaves of strongly folded amphibolitic gneiss in which the gneissic layering preserved in sample THG2 is axial planar to the folds within the mafic enclaves. The mafic rafts are similar in appearance to amphibolite units in the Corella Formation.

Other two regional samples (THG4, MG) are from variably foliated, late tectonic intrusions, which were mapped as Tick Hill Granite and emplaced into strongly sheared and folded ($D_{1\text{-}2}$) mylonitic gneiss mapped as Corella Formation. These samples were taken to constrain the minimum age of $D_{1\text{-}2}$ deformation event and associated high-temperature metamorphism. Sample THG4 is foliated granite collected from a low set of hills, 3.5 km southwest of the pit and consists of a relatively undeformed leucogranite, characterized by weakly flattened quartz phenocrysts that are <5 mm in size, and partly recrystallized, slightly elongated K-feldspar grains that together with quartz define a weak foliation (Fig. 4f), which intensifies towards the margins of the intrusion. Internal to the intrusion the grainsize locally coarsens into pegmatoidal pockets that typically display graphic intergrowths between K-feldspar and quartz. The intrusion was mapped as part of the Tick Hill Complex (e.g., Wyborn, 1997), and has a sharp intrusive contact that transects $D_{1\text{-}2}$ folding in the surrounding mylonitic gneiss units. Therefore, sample THG4 represents a late-syntectonic granite relative to the dominant $D_{1\text{-}2}$ fabric and was probably emplaced late during D_2. Sample THG4 consists of quartz, plagioclase and K-feldspar with rare biotite and no other mafic phases, in which plagioclase and K-feldspar were replaced by sericite (±albite, clay minerals). Sample MG was obtained from thin (<20 cm), quartz-poor monzonite veins and dykes, that cut across intensely folded, sheared and migmatised ($D_{1\text{-}2}$) amphibolitic calc-silicate gneiss ~6 km south-southwest of Tick Hill pit (Fig. 4g,h). The dyke pinches and swells as it transects isoclinal folds and the $S_{1\text{-}2}$ layering at a 20–30° angle across platform outcrops in the river. The monzonite preserves a weak foliation and lineation (Fig. 4g,h), which is similar in orientation to the regional $L_{1\text{-}2}$, and indicates that the dyke was emplaced late during D_2. Sample MG comprises roughly equal amounts of plagioclase and K-feldspar, with biotite and amphibole and minor quartz. Plagioclase was strongly altered by sericite whilst biotite was replaced by chlorite.

3.2. Local samples

The first groups of local samples in Tick Hill include one sample of mylonitic, syn-tectonic granite mapped as Tick Hill Granite (sample THG3) and two samples of gold-rich quartz-feldspar mylonite (galahstone) from the core of the deposit (THM04, THM27) that are hosted within rocks mapped as Corella Formation. These samples were taken to constrain the age of $D_{1\text{-}2}$ deformation event and provide a maximum age for mineralization, and a minimum age for the host rocks in which they intruded.

Table 3
Locations for all samples used in this study, together with a summary of the U-Pb zircon $^{207}Pb/^{206}Pb$ ages for key stratigraphic units in the Tick Hill region. The ages are based on weighted mean averages of grains with < 10% discordance. Errors are shown as 2σ; photos and plots are shown in Figs. 10 to 18.

Mapped rock unit (Fig. 1)		Sample ID	Location	Zone 54-GDA94		Age (Ma)	Age comment
				East (m)	North (m)		
Pre-D_1	One Tree granite	OTG	10 km W of Tick Hill	378,568	7,602,967	1857 ± 5	n = 20; MSWQ = 0.96
	Saint Mungo granite	THG2	3,7 km W of Tick Hill	385,138	7,606,776	1850 ± 6	n = 10; MSWD = 1.6
Syn-D_1	Saint Mungo granite	SMG	8 km W of Tick Hill	381,233	7,604,274	1790 ± 7	n = 21; MSWD = 0.42
	Tick Hill granite	THG1	3,5 km W of Tick Hill	385,156	7,606,851	1777 ± 3	n = 38; MSWD = 1.04
Syn-$D_{1\text{-}2}$	Tick Hill granite	THG4	3,5 km SW of Tick Hill	386,702	7,603,938	1777 ± 14	n = 1
	Tick Hill granite	THG3	0,5 km E of Tick Hill	389,258	7,605,939	1778 ± 10	n = 7; MSWD = 1.5
	Tick Hill quartz-feldspar mylonite	THM27	Tick Hill, underground	388,842	7,605,934	1771 ± 5	n = 43; MSWD = 0.82
	Tick Hill quartz-feldspar mylonite	THM04	Tick Hill, underground	388,850	7,605,950	1789 ± 16	n = 5; MSWD = 1.18
Syn-D_2	Monzonite dyke	MG	23 km SSW of Tick Hill	386,650	7,600,566	1773 ± 7	n = 8; MSWD = 1.2
Syn-D_3	Tick Hill syn-D_3 pegmatite (possibly syn-D_2)	TH11	Tick Hill pit	388,869	7,605,868	1772 ± 19	n = 4; MSWD = 2.1
	Tick Hill syn-D_3 pegmatite	TH141	Tick Hill pit	388,867	7,606,015	1522 ± 3	n = 81; MSWD = 0.79
	Tick Hill syn-D_3 pegmatite	TH108	Tick Hill, DH U8506: 224–224.3 m; 236.5–236.8 m; 240.3–240.5 m;	388,728	7,605,910	1524 ± 6	n = 27; MSWD = 1.14
	Tick Hill syn-D_3 pegmatite	TH140	Tick Hill, DH TH032: 285.5–286.1 m	388,607	7,605,915	1530 ± 19	n = 3; MSWD = 0.2
	Tick Hill syn-D_3 pegmatite	TH66	Tick Hill, DH U9205: 149.45–149.9 m	388,752	7,605,976	1517 ± 45	n = 3; MSWD = 0.021
Pre- or syn-D_1?	Hangingwall quartzite	TH13	Tick Hill pit	388,842	7,605,827	1781 ± 6	n = 19; MSWD = 1.2
	Footwall quartzite	TH01	Tick Hill pit	388,913	7,605,912	1841 ± 15	n = 11, MSWD = 0.74
Syn-$D_{1\text{-}2}$	Monument syenite	Msy	6.1 km SSW of Tick Hill	386,953	7,600,313	Whole rock geochemistry only	
	Monument syenite	Msy.m	6.1 km SSW of Tick Hill	386,914	7,600,329		
	Syenite dyke	Msy.d	6.1 km SSW of Tick Hill	386,953	7,600,313		
Syn-D_3	Tick Hill post-D_3 pegmatite	TH87	Tick Hill, underground; DH U8506: 144.1–144.4 m	388,728	7605910		

Sample THG3 was collected from strongly deformed leucogranite belonging to the Tick Hill Complex at the foot of the hill, 300 m east of Tick Hill pit. It consists of mylonitic, quartzo-feldspatic gneiss that is intercalated with the surrounding metasediments (Fig. 5a) as a result of intense $D_{1\text{-}2}$ deformation (Le et al., 2021). The rock comprises granoblastic quartz, plagioclase, and K-feldspar (now largely replaced by albite) and is characterized by well-developed quartz ribbon grains, and a strong lineation defined by feldspar-quartz rodding. The outcrop from which sample THG3 was taken is part of a larger lensoidal granite body that displays strain gradients, with less intensely mylonitised granite towards its core, i.e. the rock is interpreted as a syn-tectonic intrusive leucogranite that was emplaced into the surrounding metasediments during D_1. Sample THG3 was collected to obtain an age of granite emplacement and concomitant D_1 shearing. Plagioclase was strongly altered by albite, K-feldspar and sericite.

Samples THM04 and THM27 of gold-rich, quartz-feldspar mylonite (galahstone) that constitute the principle host rock to mineralization were provided by MIM and Nick Oliver. These samples were collected from the high-grade mineralized zone at the time of mining and the exact location of the samples is not known. The two samples are near identical in composition and consist of metasomatized quartzo-feldspathic mylonite with a composite $S_{1\text{-}2}$ foliation characterized by quartz and feldspar ribbon grains (Fig. 5b,c) similar to sample THG3, but more strongly altered. The samples are dominated by quartz, K-feldspar and plagioclase with few dark minerals, most of which formed during various stages of alteration events (i.e., amphibole, chlorite, epidote and hematite). K-feldspar and plagioclase were largely replaced by albite, which in turn is generally strongly altered to sericite (+clay minerals), and the both samples contained abundant gold. The rock is characterized by a sugary, granoblastic texture reflecting post-deformational annealing and recovery (Fig. 5b,c; Le et al., 2021).

The second group of local samples are post-tectonic (i.e., syn-D_3) pegmatite veins and associated metasomatic overgrowths in the pit walls (samples TH11, TH141,) and in drill core (samples TH66, TH140, TH108). These veins are weakly deformed and undeformed, overprint the mylonitic $D_{1\text{-}2}$ fabric, and are interpreted to be emplaced during D_3 at the time of main stage of mineralization (Le et al., 2021). Sample TH141 was taken from a felsic pegmatite vein in the north wall of the pit, where it transects the dominant composite $S_{1\text{-}2}$ fabric in biotite-chlorite schist at a low angle across sharp intrusive boundaries (Fig. 5d). The pegmatite intruded along the main D_3 shear zone that forms the host to mineralization (Le et al., 2021), and is associated with an array of en-echelon quartz veins consistent with a normal-sinistral sense of movement (Fig. 5d; Le et al., 2021), i.e. the pegmatite will provide an age for D_3 normal faulting. Sample TH141 is not foliated and largely consists of coarse-grained albite and K-feldspar with subordinate quartz and minor biotite. Much of the feldspar was strongly altered to albite, epidote, sericite and clay minerals while biotite was replaced by chlorite. Sample TH11 was collected from a weakly-deformed and partly boudinaged granitic pegmatite that intruded into the $S_{1\text{-}2}$ mylonitic fabric in the east wall of the Tick Hill pit in the footwall to the mineralization (Fig. 5e). The pegmatite preserves a weak foliation defined by biotite and is dominated by feldspar with subordinate quartz (including minor quartz veins inside the feldspar-rich groundmass), biotite and traces of magnetite. The feldspar was strongly altered to sericite, albite and clay minerals while the magnetite was altered to hematite. Samples TH66

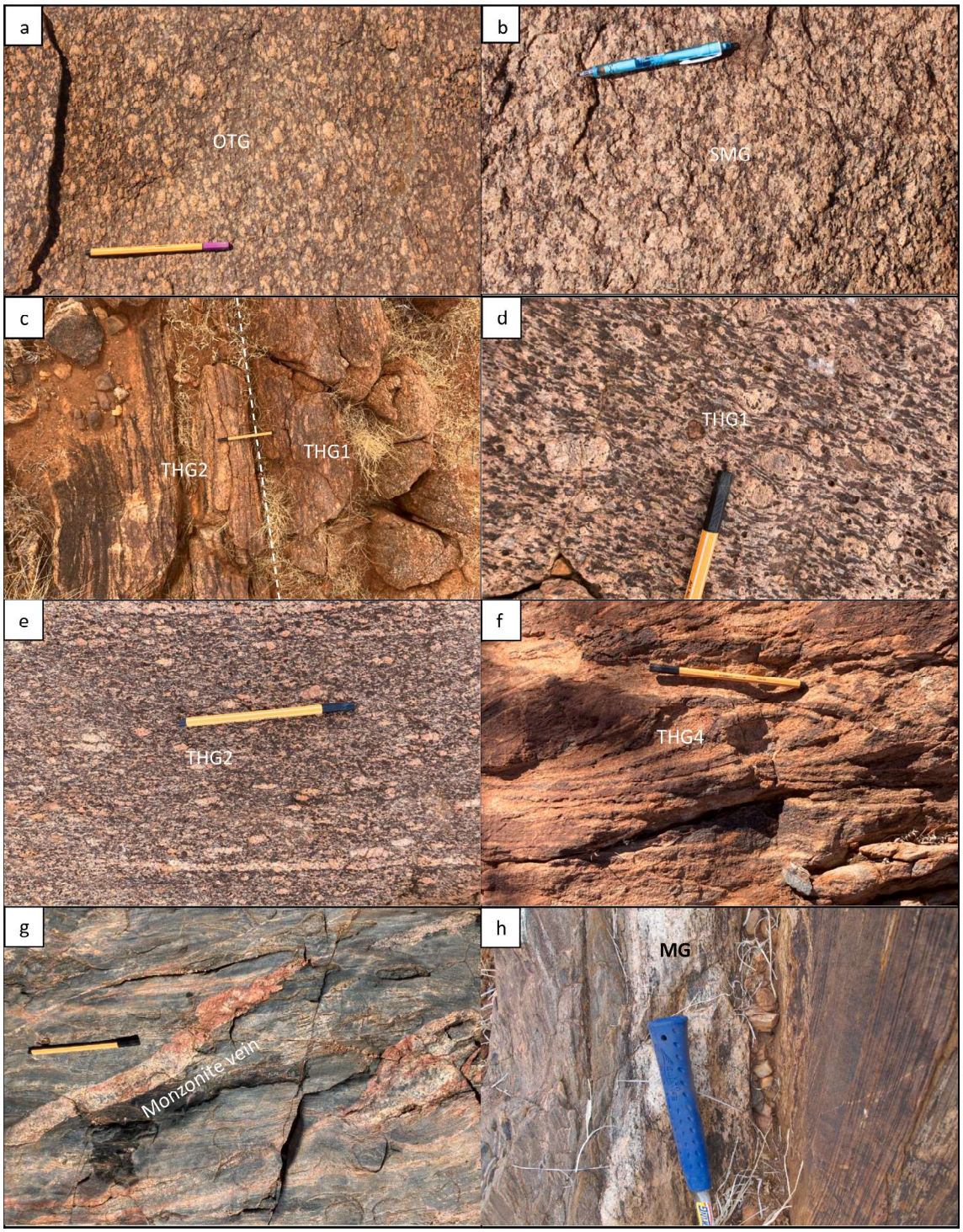


Fig. 4. Photographs of samples collected from different intrusive units in the Tick Hill region: (a) Foliated granodiorite of One Tree Granite (sample OTG); (b) Foliated granodiorite of Saint Mungo Granite (sample SMG); (c) Contact of granitic dyke (sample THG1) and older granite (sample THG2); (d) Strongly foliated granite (sample THG1) mapped as either Saint Mungo Granite or Tick Hill Granite; (e) Foliated granite (sample THG2), which was intruded by THG1 and was mapped as either Saint Mungo Granite or Tick Hill Granite; (f) Foliated late-tectonic leucogranite mapped as Tick Hill Granite (sample THG4); (g and h) Late tectonic, monzonite vein and dyke (bottom right), which intruded strongly foliated calc-silicate and amphibolite gneiss (sample MG).

(Fig. 5f), TH108 (Fig. 5g) and TH140 (Fig. 5h), were collected from drill core. All samples were taken from pegmatite dykes and metasomatic veins that truncate and overprint the footwall sequence between 80 and 180 m below the mineralized zone. Sample TH108 combines three separate intersections of post-tectonic pegmatite with similar compositions (feldspar-quartz) and textures (fine grained, non-foliated), sampled across a 16 m interval. The three pegmatite samples consist of medium-grained plagioclase and K-feldspar with minor quartz and biotite. The boundaries of the veins are generally diffuse, with feldspar-quartz overprinting and seemingly replacing the older gneissic fabric (Fig. 5h). The veins themselves are generally undeformed, but the feldspar in the veins was altered to sericite and albite (clay minerals) while biotite was altered to chlorite.

The last groups of local samples are hanging wall (sample TH13) and

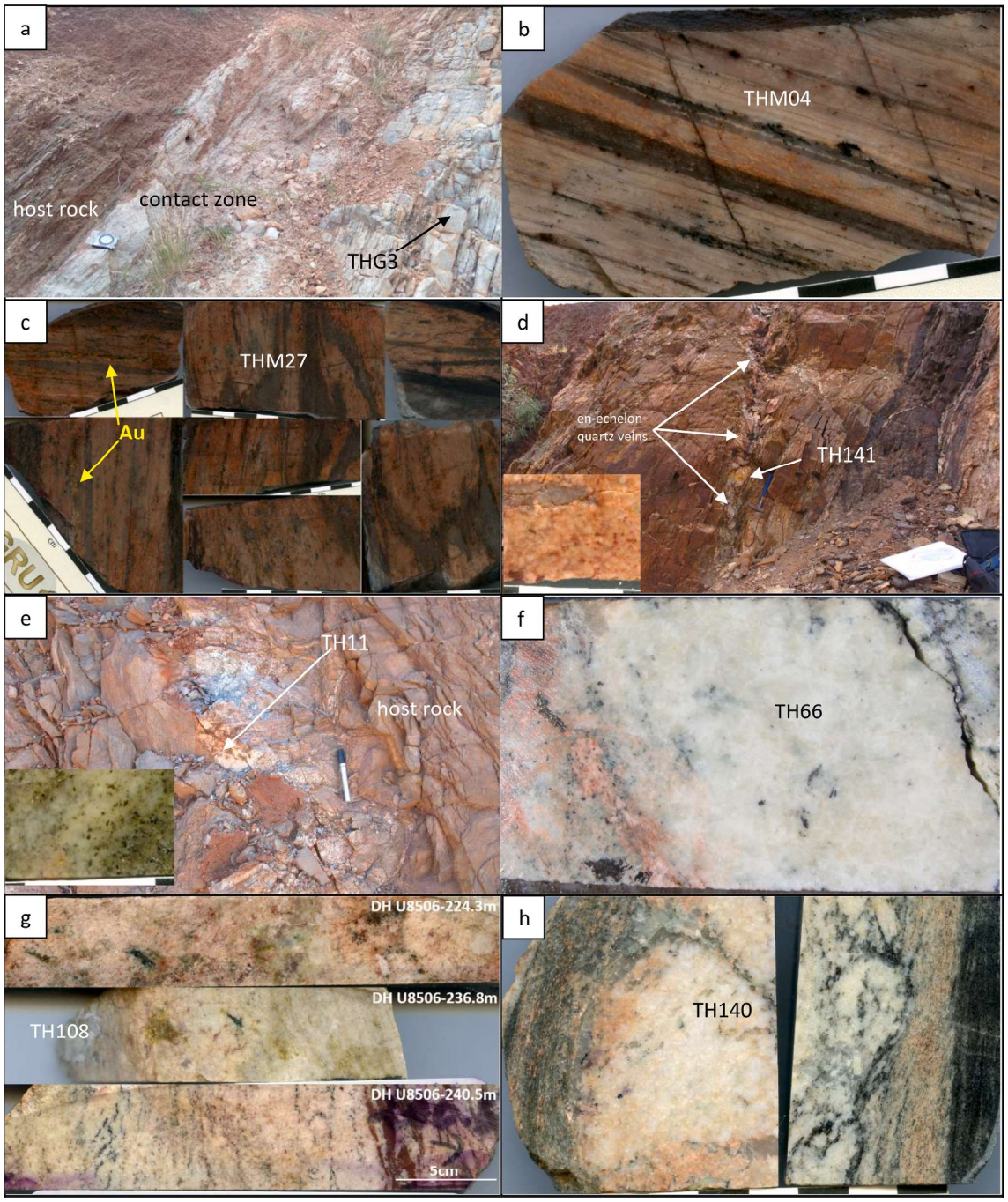


Fig. 5. Photographs of samples taken from around the Tick Hill deposit: (a) Strongly deformed (mylonitic) contact zone between syn-tectonic leucogranite (sample THG3) and gneissic host rock at Tick Hill; (b) Strongly altered, Au-rich quartz-feldspar mylonite (sample THM04); (c) Offcuts of strongly altered Au-rich quartz-feldspar mylonite (collective sample THM27); (d) Pegmatite associated with en-echelon quartz veins in the north wall of the pit (sample TH141); (e) Boudinaged pegmatite dyke in the east pit wall of the pit below the main ore zone (sample TH11); (f) Metasomatic feldspar-dominant vein underneath the Au-rich mineralization zone in DH U9205 (sample TH66); (g) Metasomatic feldspar-dominant zones overprinting gneissic layering in three intervals from DH U8506 (collectively sampled as TH108); (h) Contact of late-tectonic (D_3) pegmatite dyke (sample TH140) and host rock from drill core underneath the ore zone.

footwall (sample TH01) quartzite units that bound the ore zone in the pit. The hanging wall quartzite forms the immediate hanging wall to mineralization, and is locally mineralized. It is a composite unit that varies in thickness, and it has diffuse boundaries and significant internal lithological variation (Laing 1993; Tedman-Jones, 2001). The hanging wall contact with overlying calc-silicates is magnetite rich, whilst the main body of quartzite includes zones dominated by oriented grains of either biotite, hornblende-epidote-feldspar or altered feldspar that are aligned within S_{1-2} to resemble silicified biotite schist, calc-silicate or quartzofeldphatic gneiss respectively. The amount of biotite, hornblende, epidote and feldspar vs quartz is variable, and portions of almost pure white quartzite occur. Within the hanging wall quartzite evidence for brecciation and intense stockwork veining, now largely annealed, is common, and the unit has been variably interpreted as a primary sedimentary horizon or as alteration along a D_1 shear zone (Laing 1993; Tedman-Jones, 2001). Dates from this unit may, therefore, either provide an upper age limit for the sedimentary sequence, or an age for D_1 metasomatism. Sample TH13 was taken from hanging wall quartzite in

the southeast corner of the pit (Fig. 6a). The sample has a spotted texture as a result of abundant (~10%) feldspar grains with minor biotite that are aligned within the $S_{1\text{-}2}$ foliation, and that are largely overgrown and replaced by quartz (Fig. 6b). As such, this unit could represent strongly silicified quartzo-feldspathic gneiss. The quartz is extremely coarse-grained as a result of post-tectonic annealing and grain growth, but inclusion trails of tourmaline, amphibole, and other accessory minerals preserve evidence for the underlying older fabric. The sample was strongly metasomatised which resulted in the growth of quartz at the expense of feldspar and biotite (Fig. 6b), the replacement of feldspar by sericite and abundant fluid inclusion trails in quartz, whilst biotite was altered to chlorite.

The footwall quartzite is thickly bedded (>30 cm), and appears less deformed and altered and more quartz-rich than the hanging wall quartzite (Fig. 6c,d). Sample TH01 was collected in the northeast corner of the pit. The sample consists almost completely of grey-white translucent quartz with a little biotite and magnetite. The quartz is extremely coarse-grained (up to 1 cm) due to post tectonic annealing and D_3 metasomatism as indicated by the abundance of fluid inclusion trails along healed fractures, but the underlying gneissic fabric has been preserved by the alignment of accessory minerals. Similar to the hanging wall quartzite, the footwall quartzite was variably interpreted as a sedimentary unit or a silicified D_1 shear zone (Laing 1993; Tedman-Jones, 2001), and dates from this unit may either reflect an upper age limit for the sedimentary sequence, or an age for D_1 metasomatism.

3.3. Additional samples for geochemistry

In addition to the geochronology samples described above, a further two samples were collected from the main body of Monument Syenite *(MSy, MSy.m)* and one sample from an associated intrusive syenite dyke *(MSy.d)*, which intruded ~6 km south of Tick Hill (Fig. 3a). These samples did not yield zircon but were included for geochemical analyses. The Monument Syenite intrusions preserve a well-developed linear fabric (L-tectonite) with the lineation parallel to the regional mylonitic L_1 fabric. It consists of K-feldspar and plagioclase with little quartz and abundant magnetite. The syenite dyke is weakly foliated with a fine-grained aphanitic texture, with amphibole and magnetite in a matrix of intergrown plagioclase and K-feldspar. In addition, one further sample of undeformed, late-tectonic pegmatite was taken from drill core below the ore zone (sample TH87). This sample did not provide sufficient concordant zircon in dating, but it has been used to supplement the geochemistry data for the late pegmatite group.

4. Analytical methods

4.1. Major and trace element analyses

Intrusive rock units targeted for age dating were analyzed for major and trace element geochemistry. Selected samples were crushed and milled to powders that were fused in beads for analysis. Major elements for most samples were obtained by the Advance Analytical Centre at James Cook University, using a Bruker-AXS, S4 Pioneer XRF Spectrometer. FeO and trace elements including fluorine were analyzed at Bureau Veritas Canada Inc. in Vancouver, British Columbia, using ICP-ES/MS techniques. Both major and trace elements for samples TH140 and TH141, were analyzed at Bureau Veritas. Samples TH108 and TH87 were analyzed for major-elements only. Major and trace element values were processed and analyzed in ioGAS software. All values below detection limits were assigned half the value of the lower detection limits. Details of the analytical methods are presented in Appendix 2.

4.2. U-Pb dating of zircon by LA-ICP-MS

Zircon grains were separated from rock powders with heavy liquid followed by hand picking under the microscope. Selected zircon grains were mounted in 2.5 cm epoxy-resin mounts, which were polished and imaged with a cathodoluminescence microscope to classify zircon types and detect internal textures (Corfu et al., 2003; Kwelwa et al., 2018).

Individual grains were analysed by LA-ICP-MS, using a Geolas Pro

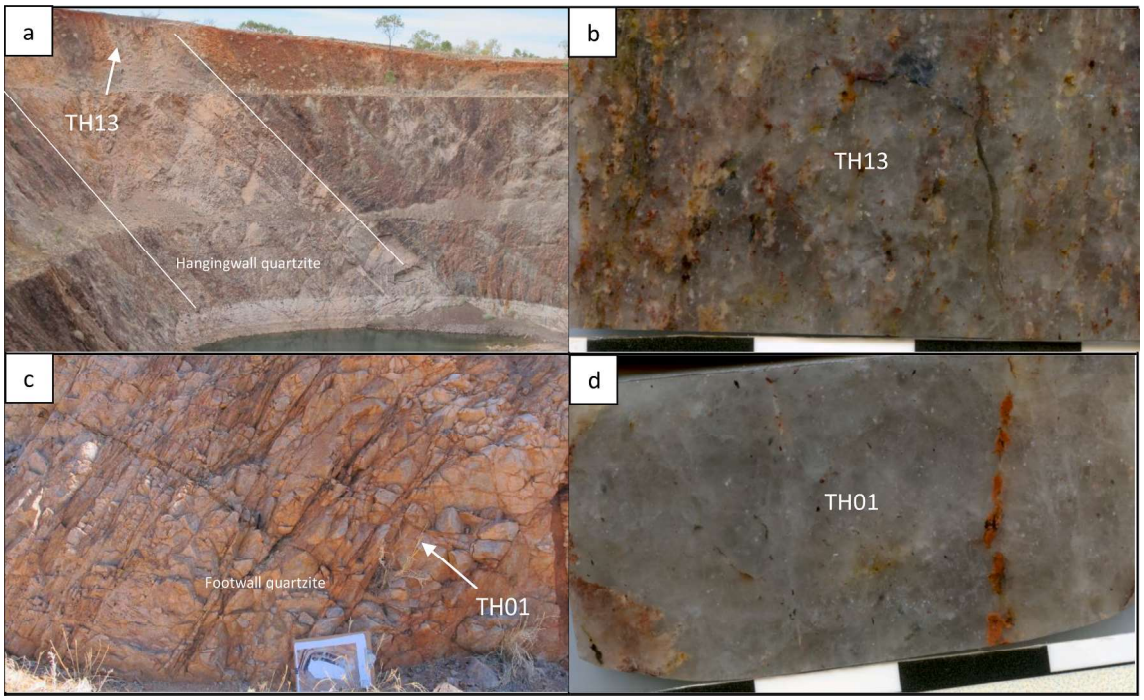


Fig. 6. Photographs of hanging wall and footwall quartzite samples taken from the open pit: (a) Hanging wall quartzite exposed in the southeast corner of the pit with the location of sample TH13 indicated. (b) Close-up of sample TH13 (scale bar in centimeters) illustrating the spotty feldspar texture, with feldspar aligned along $S_{1\text{-}2}$ and overprinted by quartz. (c) Footwall quartzite exposed in the northeast corner of the pit with the location of sample TH01 indicated. (d) Close-up of quartzite sample TH01 showing the coarse-grained recrystallized nature of quartz.

193 nm ArF excimer laser system coupled with a Bruker 820–MS ICP-MS at the Advanced Analytical Centre, James Cook University, Townsville. Ablation was conducted in a large volume cell using high-purity He as the carrier gas (Fricker et al., 2011), which was subsequently mixed with Ar prior to introduction into the ICP-MS. Full analytical details are described in Tucker et al. (2013). Analytes collected were ^{29}Si, ^{90}Zr, ^{202}Hg, ^{204}Pb, ^{206}Pb, ^{207}Pb, ^{208}Pb, ^{232}Th, ^{235}U, and ^{238}U. The ICP-MS was tuned to ensure low oxide production levels (ThO/Th < 0.5%) and approximately equal sensitivity of U, Th and Pb to minimize isotope fractionation due to matrix effects (Pettke, 2008). Fractionation and mass bias were corrected by using standard bracketing techniques with every eight to ten zircon sample measurements bracketed by measurements of GJ1 (primary calibration standard, Jackson et al., 2004), with FC1 (Paces and Miller, 1993) and 91,500 (Wiedenbeck et al., 1995) as secondary standards. All zircons were analyzed with a beam spot diameter of 25 to 36 μm depending on the size of the zircon and selection of analytical sample spots was guided by CL images. Individual analyses consist of approximately 30 s of signal of the gas background followed by 30 s of signal collected during zircon ablation. Analysis of the NIST 610 reference glass was conducted at the beginning and end of every analytical session to monitor instrument stability.

The obtained data were processed using Iolite software (Paton et al., 2011). All time-resolved single isotope signals from standards and samples were filtered for signal spikes or perturbations related to inclusions and fractures. The most stable and representative isotopic ratios were selected taking into account possible mixing of different age domains and zoning. Drift in instrumental measurements was corrected following analysis of drift trends in the raw data using measured values

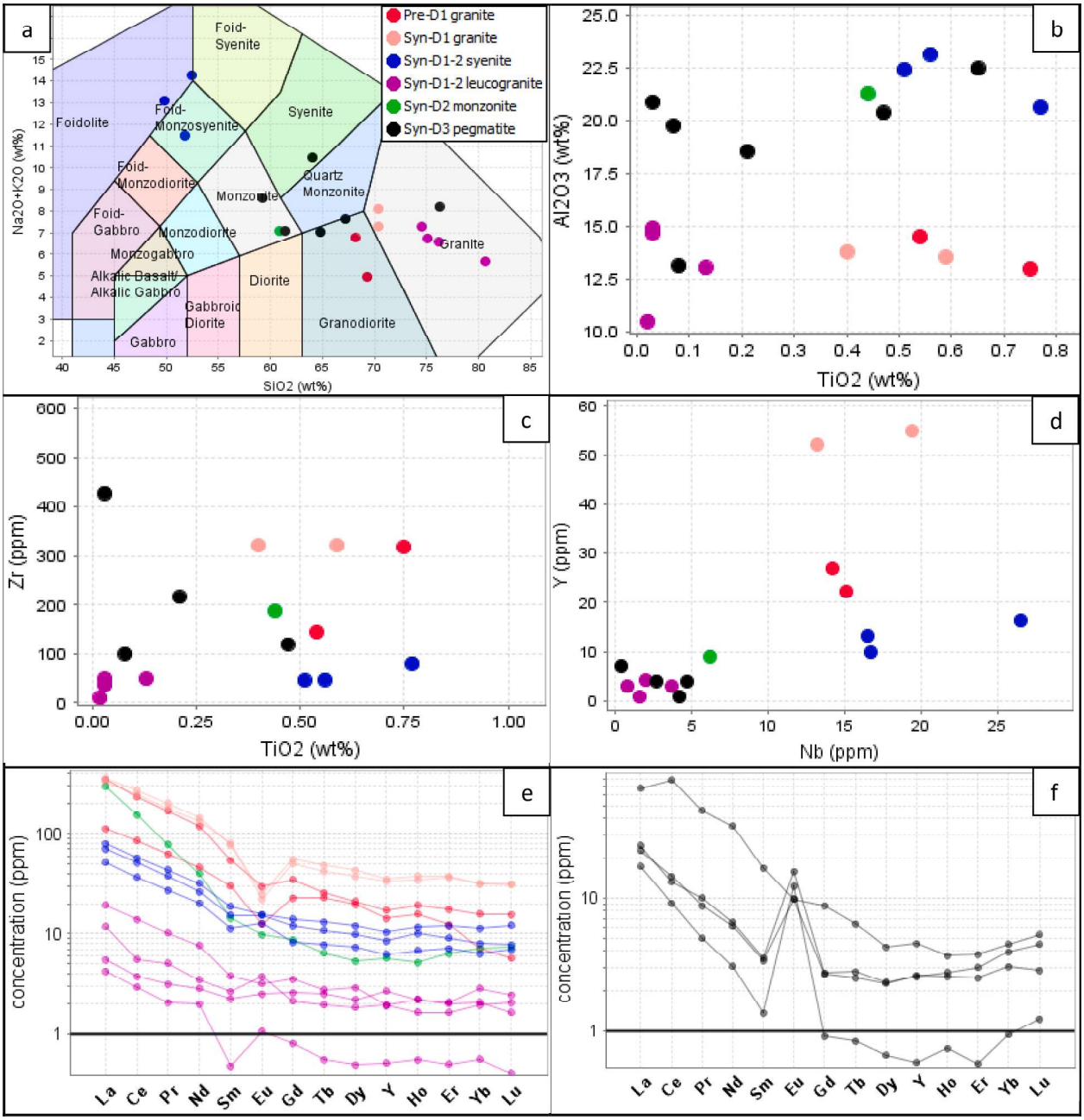


Fig. 7. Geochemical results for rocks from the Tick Hill region: (a) Rock classification diagrams (Middlemost, 1994) for major elements; (b), (c), and (d) variation diagrams of least-mobile elements including Al_2O_3 vs. TiO_2, Zr vs. TiO_2, and Y vs. Nb respectively; (e) and (f) Chrondrite-normalized REE patterns for pre-D_1 and syn-D_1 to syn-D_3 intrusions respectively. Chondrite normalization values after McDonough and Sun (1995).

for the GJ1 primary zircon standard. Age calculations based on measured isotope ratios were done for zircon grains with a discordance <10%, using Isoplot/Ex version 4.15 (Ludwig, 2011). Analyses of the secondary zircon standards were used for verification of GJ1 following drift correction. The $^{206}Pb/^{238}U$ age for the primary standard GJ1 in this study (600.24 ± 0.44 Ma; n = 322, MSWD = 0.62) was similar to ages reported by Alagna et al. (2008) and Jackson et al. (2004). The $^{207}Pb/^{206}Pb$ age for the sample FC1 (1093.2 ± 2.3 Ma; n = 146, MSWD = 0.88) is ~0.5% younger than the age reported by Paces and Miller (1993) whilst the $^{207}Pb/^{206}Pb$ age for 91,500 (1048.5 ± 3.6 Ma; n = 210, MSWD = 0.48) is ~1.5% younger than the age reported by Wiedenbeck et al. (1995).

5. Results

5.1. Whole rock geochemistry

Whole rock geochemistry results are summarized in Table 1, with various rock classification plots shown in Figs. 7 and 8. Based on their relationship with deformation events and their age as reported in Table 3, the sampled intrusive rock types have been sub-divided and plotted in relation to the deformation events as: (1) pre-D1; (2) syn-D_1, (3) syn-D_1 to syn-D2; and (4) syn-D_3 intrusions (Figs. 7 and 8).

The pre-D_1 intrusions include granite samples OTG and THG2, which were interpreted to belong to Kalkadoon basement (Blake et al., 1982; Rutherford, 2000), and contain a strong composite S_{1-2} fabric. The rocks plot in the granodiorite field (Fig. 7a), and have relatively high TiO_2 and REE values with elevated Y and MgO contents. They plot as a distinct group in the Y-Nb variation diagram (Fig. 7d), the chrondrite-

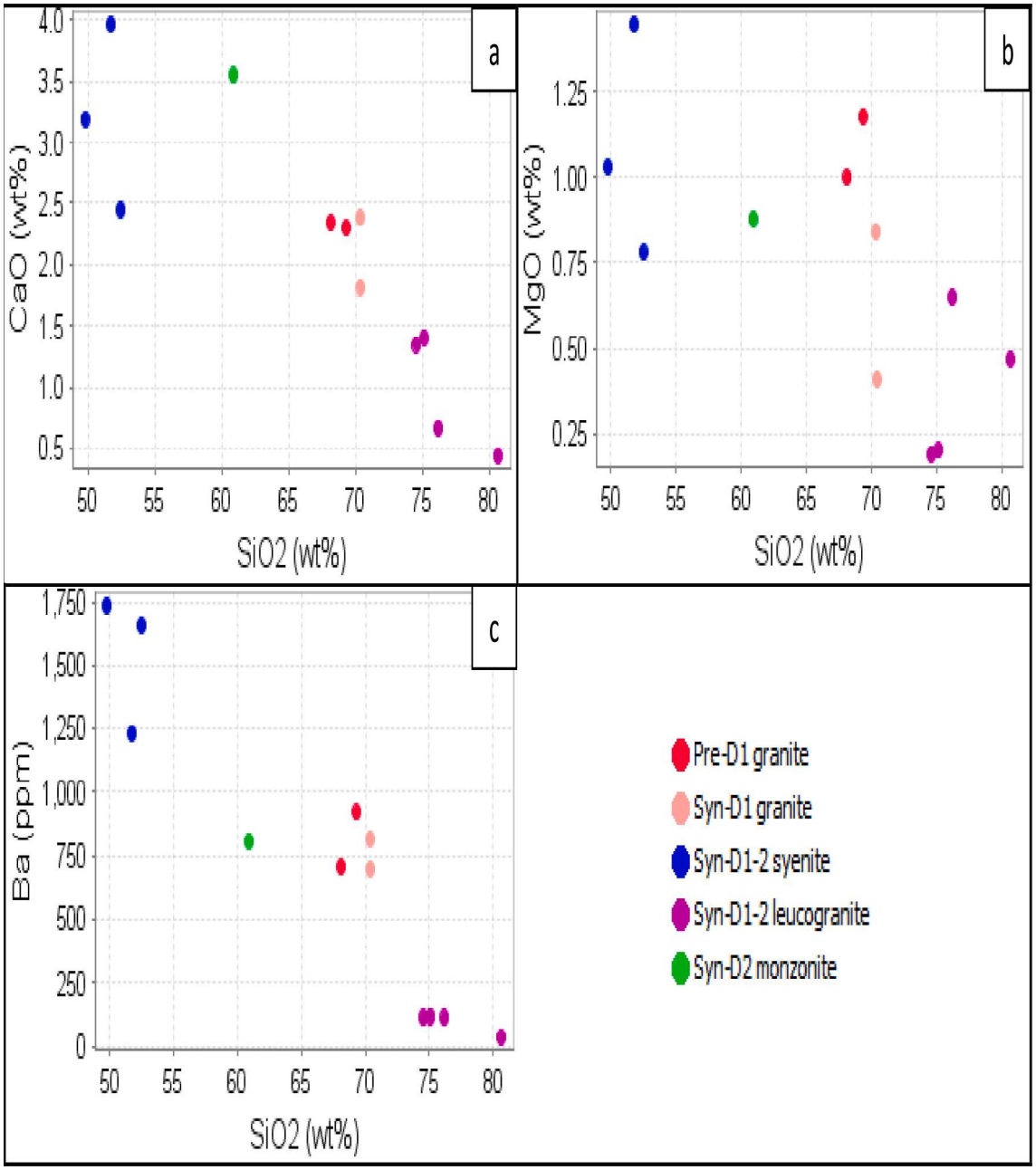


Fig. 8. Variation diagrams for SiO_2 vs. CaO (a), SiO_2 vs. MgO (b), and SiO_2 vs. Ba (c) for pre-D_1 to syn-D_2 intrusions in the Tick Hill region.

normalized REE distribution diagram (Fig. 7e), and the SiO_2 vs (Cao, MgO, Ba) diagrams (Fig. 8). Their composition is akin to the syn-D_1 granites.

Syn-D_1 intrusions include two granite samples (SMG, THG1) that have been dated and three samples of Monument Syenite (Msy, Msy.m, Msy.d) for which no dates could be obtained. Samples SMG and THG1 plot in the granite field and are broadly similar in composition to the pre-D_1 granites with which they are spatially associated (Fig. 7b, 8). The granites preserve relatively high concentrations of high-field-strength elements (HFSE) including REE, Zr and Y, and plot as a discrete group on Y-Nb and REE diagrams (Figs. 7 and 8). The syn-D_1 intrusions from the Monument Syenite form a separate group that is distinct from all other lithologies. They are silica-poor to silica-under-saturated syenite to monzosyenite (Fig. 7a) with relatively high Al_2O_3, TiO_2, CaO, Nb, Na, Sr and Ba contents (Fig. 7b,d, Fig. 8), intermediate REE enrichment, and a relatively flat REE pattern without a negative Eu anomaly (Fig. 7e).

The late syn-D_1 and syn-D_2 intrusions include the monzonite dyke sample (MG), variably deformed leucogranite samples (THG3, THG4), and gold-bearing quartz-feldspar mylonite samples (THM04 and THM27). The composition and texture of quartz-feldspar mylonite is similar to that of the leucogranite, and consequently it is grouped with the leucogranite unit. The four leucogranite samples are relatively quartz-rich and plot in the granite field (Fig. 7a). They form a discrete group in all variation diagrams (Figs. 7 and 8). The rocks are depleted in REE with relatively flat chondrite normalized distribution patterns and only minor enrichment of LREE with no clear Eu anomaly. They are also low in incompatible LILE (K, Ba, Rb Cs) and HFSE (Al, Ti, Zr, Y, Nb and Hf, Fig. 5), and they are relatively enriched in Na and depleted in Ca and K reflecting the abundance of albite in these rocks (Fig. 8, Table 1). The syn-D_2 monzonite dyke (sample MG, Fig. 7a) is enriched in LILE except

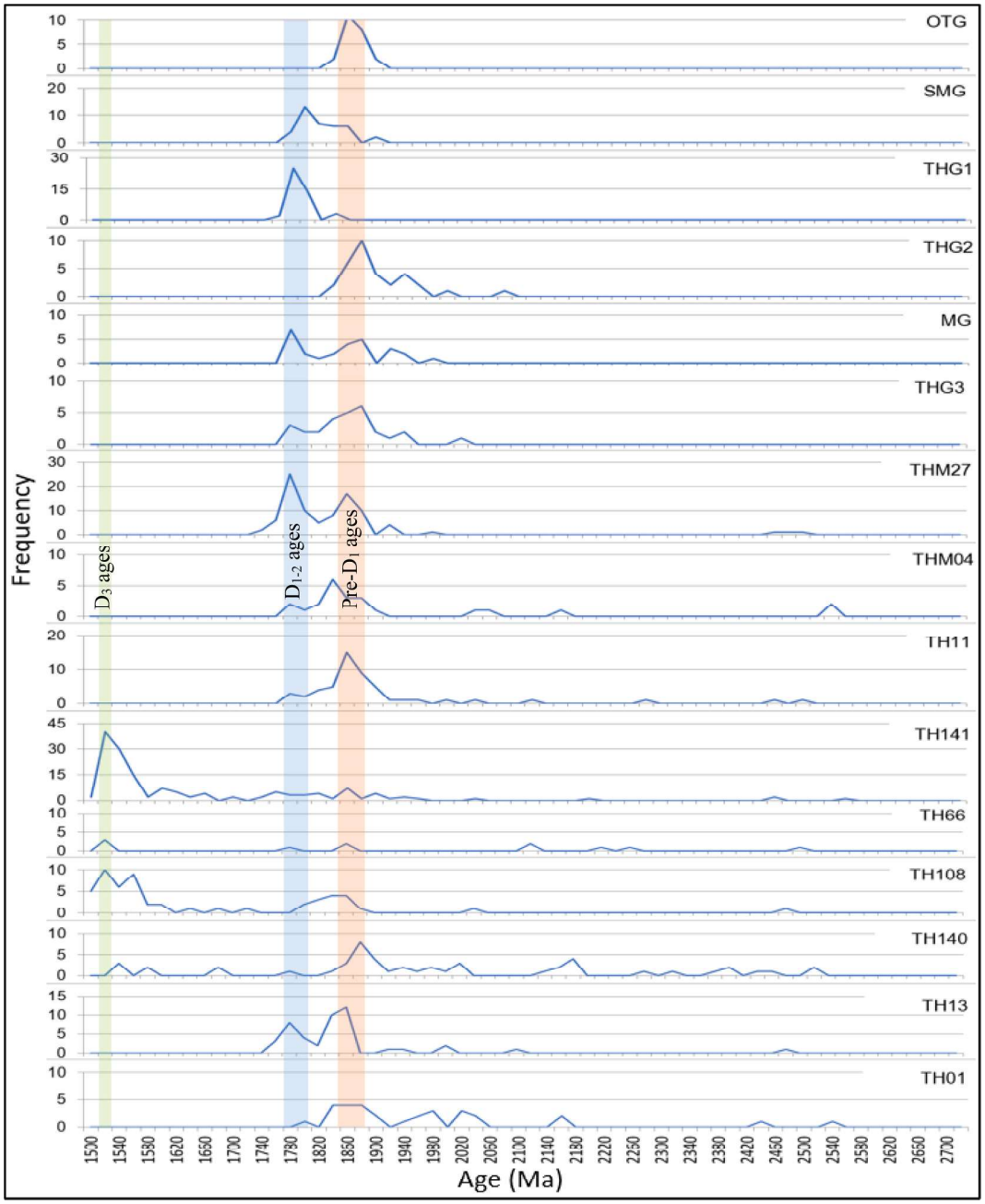


Fig. 9. Frequency plots showing near-concordant and concordant ages (Ma) for samples from the Tick Hill region. Bin sizes are 20 Ma with the age label for each bin corresponding to the middle age of the bin. Major tectonic events are indicated as coloured bars.

for Sr, and strongly enriched in U and Th (Table 1). The sample has a distinct REE pattern with strong enrichment in LREE (Fig. 7e), but with a relatively low phosphate content. It is relatively enriched in Al_2O_3, MgO, CaO, Zr, Rb, Hf and Ba (Fig. 7b,c, Fig. 8a, Table 1).

The syn-D_3 intrusions include all the late-tectonic pegmatites. These form a distinct group with variable compositions and trace element patterns. Compositionally they vary from quartz-monzonite and syenite to granite, with strong enrichment in Na (Table 1). Some samples consist of coarse-grained pegmatite, and their compositional variation is most likely due to the fact that they were incompletely sampled. Nevertheless, the pegmatites plot close together on the Nb-Y diagram (Fig. 7d) and show distinct REE patterns with positive Eu anomalies.

5.2. Geochronology

The geochronological results are summarized in the Table 3 and Fig. 9, and shown for the individual samples in Figs. 10–17. The details for each analysis, including standard analysis is presented in the Appendix 3 while the CL images for dated zircons are presented in Appendix 4. All reported ages are based on the weighted mean age of the youngest distinct age group in each sample, and only includes zircon ages that are <10% discordant. All reported error margins are given as 2σ.

5.2.1. Regional samples

Zircon grains from the pre-D_1 granite sample OTG are euhedral with prismatic to needle-like shapes. About 70% of zircon grains are dominated by metamict zircon domains with a relatively uniform texture, with the remainder being unaltered zircon domains with well-developed growth zoning (Fig. 10a). Some grains have metamorphic overgrowths that are generally irregular in outline and too narrow to be measured by LA-ICP-MS (Fig. 10a). A total of 37 analyses were conducted on unaltered and the least metamict zircon domains, that yield a single cluster of concordant ages with a weighted mean age of 1857 ± 5 Ma (n = 20, MSWD = 0.96, Fig. 10c), interpreted as the age of emplacement of the granite. Two inherited zircon grains yield near-concordant ages of 1882 ± 22 Ma and 1895 ± 25 Ma.

Sample SMG of syn-D_1 granite contains largely unaltered, zoned prismatic zircon grains of magmatic origin that are up to 500 μm in length (Fig. 10d, Corfu et al., 2003). Some are slightly metamict with thin overgrowths of hydrothermal/metamorphic zircon (Fig. 10d, Corfu et al., 2003). Only unaltered or slightly metamict zircon domains were

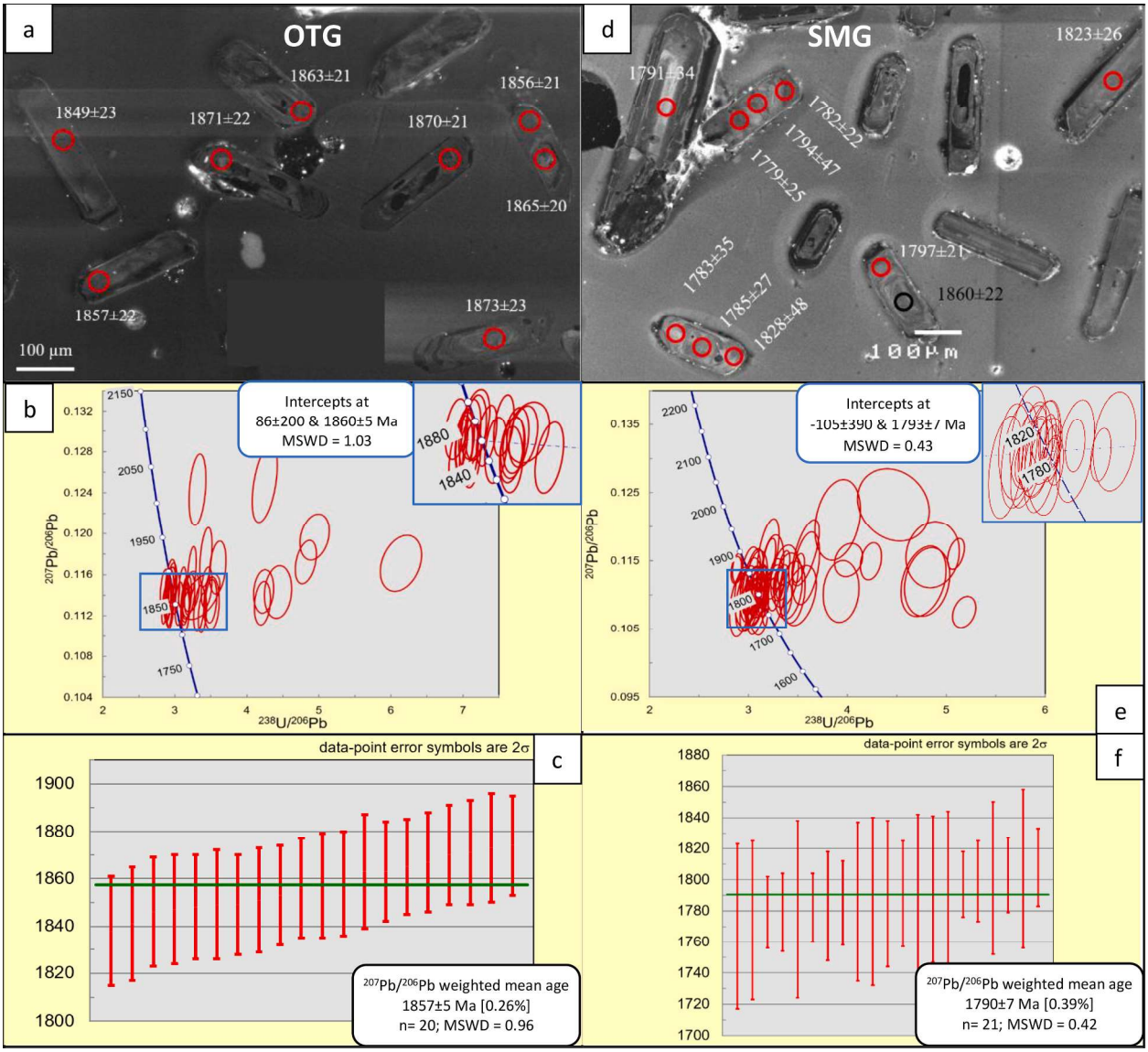


Fig. 10. Cathodoluminescence images for zircon grains from the youngest age group, concordia diagrams for all analyses, and concordant grains in the youngest age group (inset), and weighted mean age diagram for the youngest zircon group for samples OTG (a, b, and c, respectively) and SMG (d, e, and f, respectively).

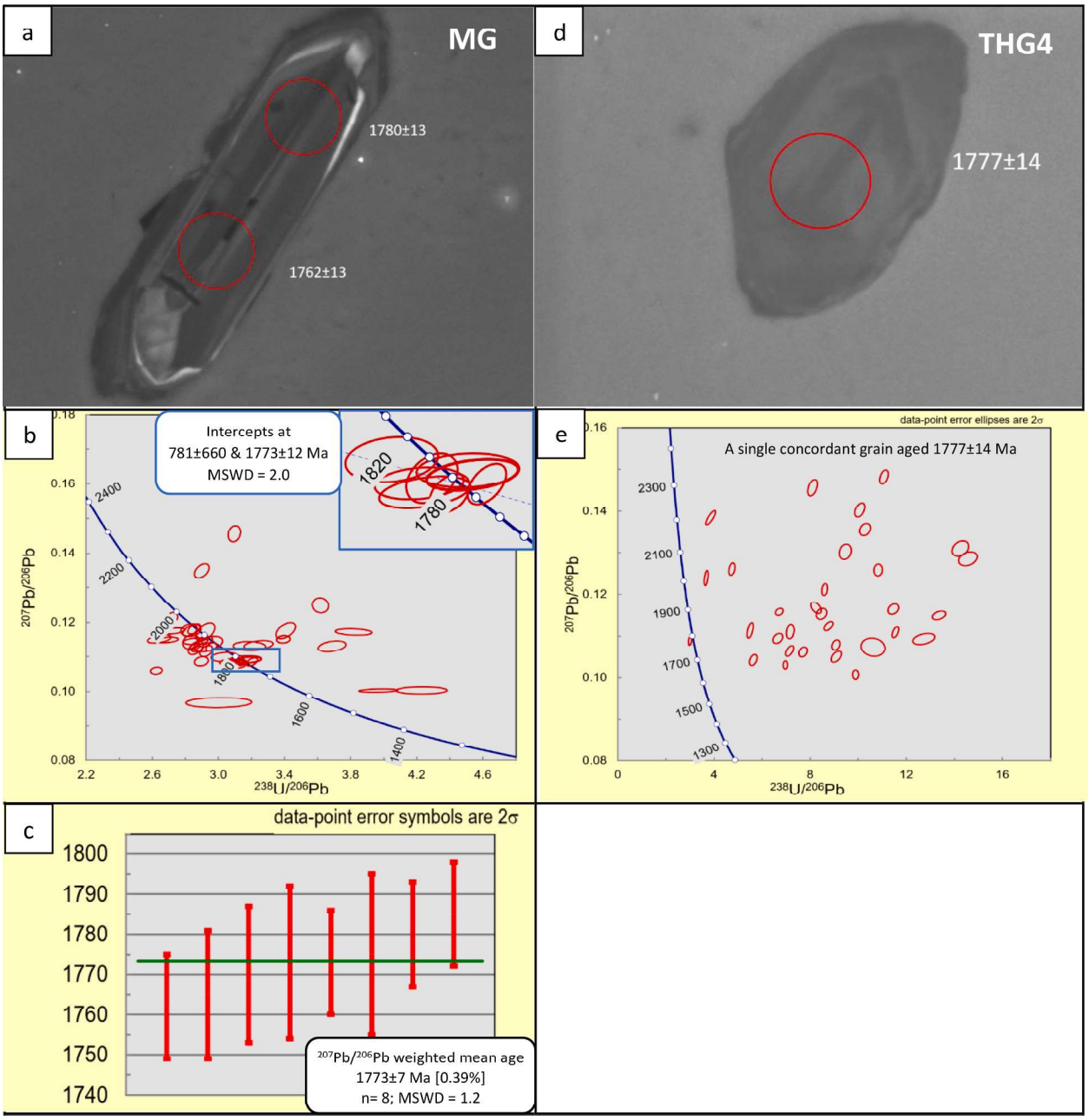


Fig. 11. Cathodoluminescence images for zircon grains from the youngest age group, concordia diagrams for all analyses and concordant grains in the youngest age group (inset), and weighted mean age diagram for the youngest zircon group for samples THG1 (a, b, and c, respectively) and THG2 (d, e, and f, respectively).

analyzed, whilst metamorphic rims were too thin to be measured. A total of 53 analyses yield three discrete age populations, with a weighted mean ages of 1790 ± 7 Ma (n = 21, MSWD = 0.42, Fig. 10f), 1826 ± 9 Ma (n = 11, MSWD = 0.77) and 1865 ± 11 Ma (n = 6, MSWD = 0.82). The youngest age is interpreted as the magma emplacement age, whilst the older age groups probably reflect inheritance.

Sample THG1 of syn-$D_{1\text{-}2}$ granite contains zircons that are similar in morphology to those described for SMG (e.g., Fig. 11a). A dominant population of concordant ages with a weighted mean of 1777 ± 3 Ma (n = 38, MSWD = 1.04, Fig. 11b,c), was obtained from a total of 53 analyses, and has been interpreted as the magmatic emplacement age. A further five concordant zircon grains yield age groupings at 1796 ± 12 Ma (n = 2, MSWD = 0.00) to 1834 ± 11 Ma (n = 3, MSWD = 0.14), interpreted to reflect inheritance.

Sample THG2 of pre-D_1 granite yielded a morphologically similar sample of zircons as OTG, with both metamict and zoned zircon grains, some with thin metamorphic overgrowths (Fig. 11d). A total of 77 analyses provided a weighted mean age for the youngest population group of 1850 ± 6 Ma (n = 10, MSWD = 1.6, Fig. 11f). This age has been interpreted as the magma emplacement age. Inherited concordant zircon grains in this sample yield two main groupings at 1876 ± 6 Ma (n = 12, MSWD = 1.6) and 1925 ± 11 Ma (n = 7, MSWD = 1.7) and three single ages ranging from 1947 ± 14 Ma to 2064 ± 18 Ma (Fig. 11e).

Syn-D_2 monzonite sample MG contains well-zoned prismatic zircons that are locally metamict with minor metamorphic/hydrothermal overgrowths (e.g., Fig. 12a). A total of 46 analyses from unaltered and metamict zircon grains, provide a weighted mean age of 1773 ± 7 Ma (n = 8, MSWD = 1.2, Fig. 12c) for the youngest group of concordant zircon grains (Fig. 12b), which has been interpreted as the age of emplacement of the monzonite dyke. An additional 18 concordant analyses define three further age groupings at 1842 ± 8 Ma (n = 9, MSWD = 1.3), 1874 ± 7 Ma (n = 3, MSWD = 0.41) and 1918 ± 8 Ma (n = 5, MSWD = 0.29),

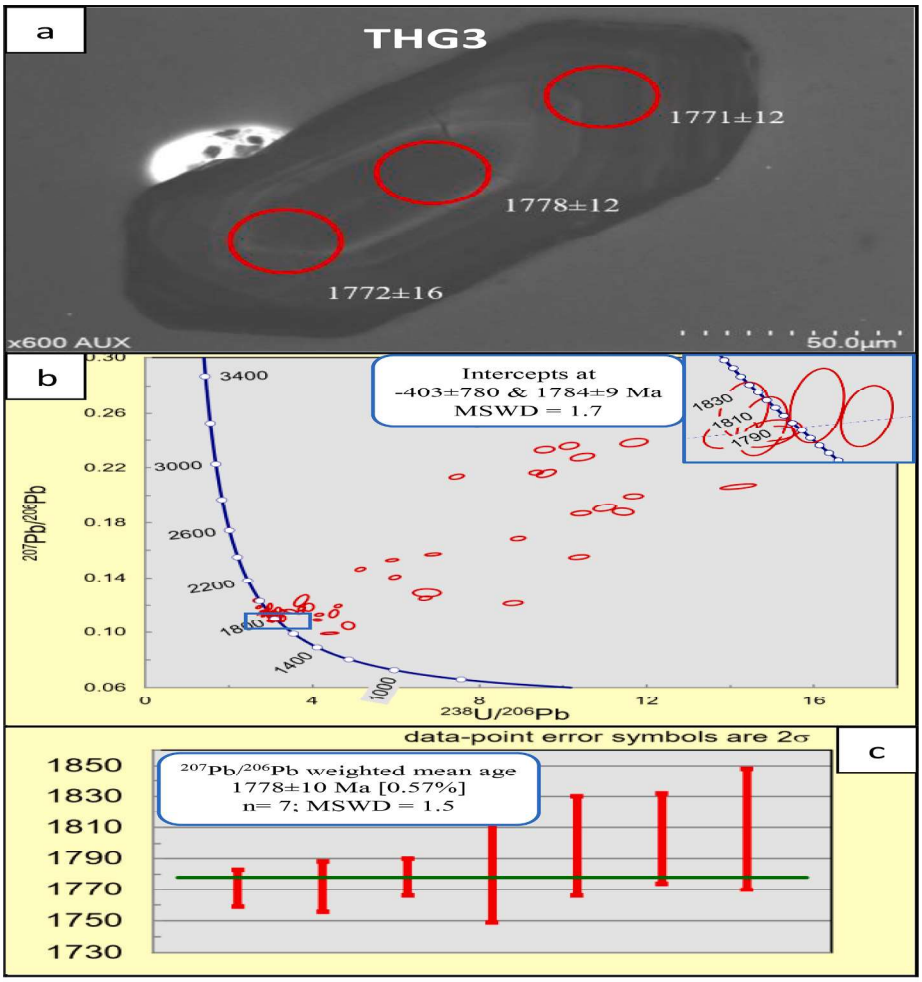


Fig. 12. Cathodoluminescence image for a representative zircon grain from the youngest age group, concordia diagram for all analyses and concordant grains in the youngest age group (inset), and weighted mean age diagrams for the youngest zircon group for sample MG (a, b and c respectively). Cathodoluminescence image and the concordia diagram of the only concordant zircon grain for sample THG4 are shown in (d) and (e).

interpreted to reflect inheritance.

Almost all zircon grains in the syn-D_2 leucogranite sample THG4 are strongly recrystallised and altered with no internal zonation (Appendix 4), and many have irregular, almost skeletal outlines suggesting partial resorption. Many of these texturally complex grains are completely metamict, and some grains preserve thin metamorphic overgrowths. Only relatively unaltered grains were sampled (Fig. 12d), and 34 analyses produced a single concordant age of 1777 ± 14 Ma (Fig. 12e), interpreted as the age of granite emplacement.

5.2.2. Local samples

Most zircon grains in the syn-D_1-$_2$ leucogranite sample THG3, were strongly recrystallised and altered (Appendix 4), and many have irregular, almost skeletal outlines suggesting partial resorption, rendering the zircons with complex internal textures that have destroyed all evidence of earlier zoning. Some grains preserve thin metamorphic overgrowths. The strongly recrystallized, metamict zircon grains either do not provide a proper data signal or yield extremely discordant ages. The sample contains a small proportion of prismatic, zoned zircon grains (Fig. 13a) for which 65 analyses in a distinct young grouping yield concordant ages with a weighted mean of 1778 ± 10 Ma (n = 7, MSWD = 1.5, Fig. 13c), interpreted as the age of emplacement. An additional 21 concordant analyses for older inherited zircon grains, define an age grouping at 1848 ± 7 Ma (n = 14, MSWD = 1.09) with further ages ranging from 1875 ± 10 Ma to 1939 ± 28 Ma.

The syn-D_1-$_2$ gold-bearing quartzo-feldspathic mylonite samples TH004 and THM27, are dominated by weakly metamict zircon grains characterized by homogenized internal textures, with metamorphic rims that are too thin to measure (Fig. 14a, d). Based on 109 analyses for zircon grains from sample THM27, the youngest population of concordant ages has a weighted mean of 1771 ± 5 Ma (n = 43, MSWD = 0.82, Fig. 14c), which is interpreted as the age of emplacement of the original quartz-feldspathic leucogranite. An additional 48 concordant analyses provide a further inherited age grouping at 1845 ± 6 Ma (n = 40, MSWD = 1.2) and other ages that range from 1915 ± 17 Ma (n = 4, MSWD = 0.08) to 2473 ± 48 Ma (n = 3, MSWD = 2.2). The youngest age grouping for concordant zircon grains from 38 analyses for sample THM04 provides a weighted mean age of 1789 ± 16 Ma (n = 5; MSWD = 1.18, Fig. 14f), again interpreted as the age of emplacement of the original quartz-feldspathic leucogranite. An additional 15 inherited concordant grains yield a cluster at 1848 ± 9 Ma (n = 13, MSWD = 0.96) with further ages ranging from 2036 ± 24 Ma (n = 2, MSWD = 0.61) to 2530 ± 22 Ma (n = 2, MSWD = 0.00).

The syn-D_3 pegmatite samples (TH11, TH141, TH66, TH108 and TH140) yield complex zircon populations dominated by hydrothermal zircon characterized by a framework texture of bright seams surrounding black domains (e.g., Fig. 15d). Other zircon grains show partly zoned and metamict domains, locally recrystallized and overgrown by zircon domains with complex framework textures (e.g., Fig. 15a) that indicates hydrothermal and metamorphic zircon. Analyses of metamorphic zircon domains yielded only discordant ages. Hydrothermal and metamict zircon domains in each of the samples provided similar ages. In sample

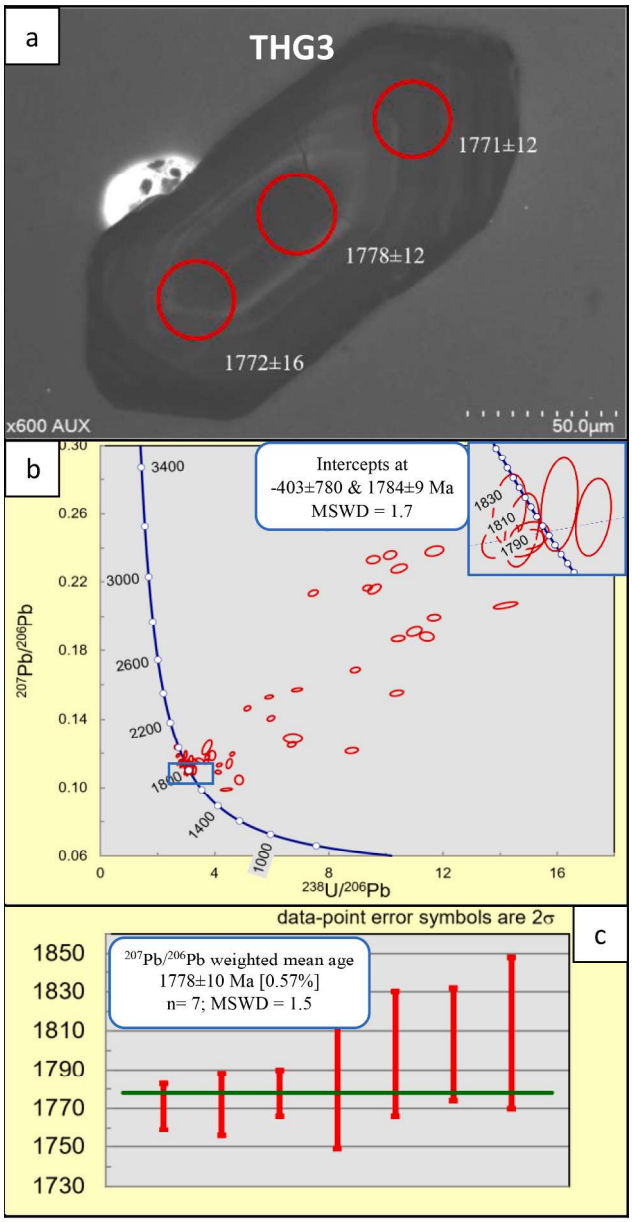


Fig. 13. Cathodoluminescence image for a representative zircon grain from the youngest age group, concordia diagram for all analyses, and concordant grains in the youngest age group (inset), and weighted mean age diagrams for the youngest zircon group for sample THG3 (a, b, and c, respectively).

TH11, 87 analyses for the least altered zircons (i.e., metamict zircon domains with homogenous texture, Fig. 15a) provide a large spread of ages, reflecting inheritance. The youngest four concordant grains provide a weighted mean age of 1772 ± 19 Ma (n = 4, MSWD = 2.1, Fig. 15c), but it is not clear if this age whether represents an emplacement age or reflects inheritance from the surrounding gneiss units because the sample is considered as syn-D_3 pegmatite based on its texture and geochemical signatures as being discussed above. A further 48 concordant analyses from TH11 provided three distinct age groupings at 1824 ± 11 Ma (n = 8, MSWD = 2), 1854 ± 4 MA (n = 21, MSWD = 0.67) and 1883 ± 7 Ma (n = 10; MSWD = 0.64), and additional individual ages that range from 1924 ± 24 to 2498 ± 11 Ma (n = 8, Fig. 15b). Sample TH141, with 219 analyses (of which 150 were concordant) mostly taken from hydrothermal zircon and metamict zircon provided a weighted mean age of 1522 ± 3 Ma (n = 81, MSWD = 0.79, Fig. 15f) for the youngest grouping of concordant zircon grains. This age is well constrained and has been interpreted as the age of pegmatite emplacement and related hydrothermal events during D_3. Other groupings of (near-)concordant analyses for hydrothermal zircons provide mean ages of 1557 ± 11 Ma (n = 8, MSWD = 0.075), 1602 ± 8 (n = 11; MSWD = 0.6), 1649 ± 16 Ma (n = 4; MSWD = 0.083), 1743 ± 12 Ma (n = 7, MSDW = 0.8), 1788 ± 13 Ma (n = 8, MSWD = 0.99), 1841 ± 12 Ma (n = 9; MSWD = 0.79), 1880 ± 12 (n = 7, MSWD = 1.05), with an additional eight analyses yielding individual ages of between 1922 ± 28 Ma and 2558 ± 34 Ma.

Sample TH66 with 28 analyses from hydrothermal and metamict zircon (Fig. 16a), provided a weighted mean age of 1517 ± 45 Ma (n = 3; MSWD = 0.021, Fig. 16c) for the youngest three concordant analyses of hydrothermal zircon, which is interpreted to approximate the hydrothermal age and probably also the pegmatite emplacement age. Another eight concordant grains provide inherited ages ranging from 1796 ± 74 Ma to 2496 ± 96 Ma. Sample TH108 (121 analyses) from hydrothermal and metamict zircon (Fig. 16d), yielded a weighted mean age of 1524 ± 6 Ma (n = 27; MSWD = 1.14, Fig. 16f) for the youngest population of concordant zircon grains. This age has been interpreted as the age of pegmatite emplacement and associated hydrothermal events during D_3. An additional 26 concordant ages range from 1547 ± 21 Ma to 2480 ± 72 Ma, and define three main groupings at 1557 ± 12 Ma (n = 5, MSWD = 0.55), 1795 ± 11 Ma (n = 5, MSWD = 0.6) and 1834.1 ± 10 Ma (n = 8, MSWD = 1.3), all indicative of inheritance from the surrounding host rocks. Sample TH140 (76 analyses) contains only few near-concordant grains with a weighted mean age of 1530 ± 19 Ma (n = 3; MSWD = 0.2, Fig. 17c) for the youngest three concordant grains of hydrothermal zircon. An additional five concordant analyses for hydrothermal grains yield ages between 1572 ± 32 Ma and 1675 ± 30 Ma, and another 45 concordant analyses from metamict grains give inherited ages ranging between 1777 ± 56 Ma and 3190 + 31 Ma, including four age clusters around 1869 ± 8 Ma (n = 16, MSWD = 1.12), 1948 ± 13 Ma (n = 6, MSWD = 1.07), 2008 ± 15 Ma (n = 4, MSWD = 0.3) and 2158 ± 12 Ma (n = 7, MSWD = 1.01).

Sample TH13 of hanging wall quartzite comprises zircon grains showing (sub)rounded to prismatic and needle-like shapes. Some grains preserve cores of zoned zircon or metamict domains with uniform textures, and thin metamorphic rims are common (Fig. 18a). Results for 124 analyses from elongated, euhedral to slightly anhedral prismatic grains fall into two main concordant populations with weighted mean ages of 1781 ± 6 Ma (n = 19, MSWD = 1.2, Fig. 18c) and 1841 ± 4 Ma (n = 20, MSWD = 0.98). The mean age for the youngest age grouping can be interpreted as the maximum age of quartzite deposition if the quartzite is interpreted as a sedimentary horizon. Alternatively the quartzite in sample TH13 can be interpreted as strongly silicified quartzo-feldspathic gneiss similar to quartzo-feldspathic mylonite (e.g., Laing, 1993; Tedman-Jones, 2001), in which case the age may represent the age of emplacement of an original leucogranite. The latter interpretation is more consistent with the needle-like prismatic morphology of many of the grains. An additional six concordant ages provide inherited ages that range from 1919 ± 12 Ma to 2467 ± 45 Ma.

Sample TH01 of footwall quartzite show rounded to prismatic and needle-like zircon grains (Appendix 4), with individual grains exhibiting either internal growth zoning or uniform metamict textures with concentric metamorphic domains replacing original growth zoning (Fig. 18d). Some zircon grains have thin metamorphic rims that are too thin to measure with the laser. About 10% of zircon grains from this sample are extremely metamict, leaving the grains homogenously black in color (Appendix 4). These grains do not yield any concordant ages. Results for 77 analyses for rounded to euhedral grains yielded three concordant zircon groupings with weighted mean ages of 1841 ± 15 Ma (n = 11, MSWD = 0.74, Fig. 18f), 1883 ± 24 Ma (n = 4; MSWD = 0.1) and 1984 ± 22 Ma (n = 11, MSWD = 1.7). Additional older ages for individual concordant granis range from 2146 ± 51 Ma to 2532 ± 46 Ma (Fig. 18e, f). The mean age for the youngest age grouping can be interpreted as the maximum age of quartzite deposition if the quartzite

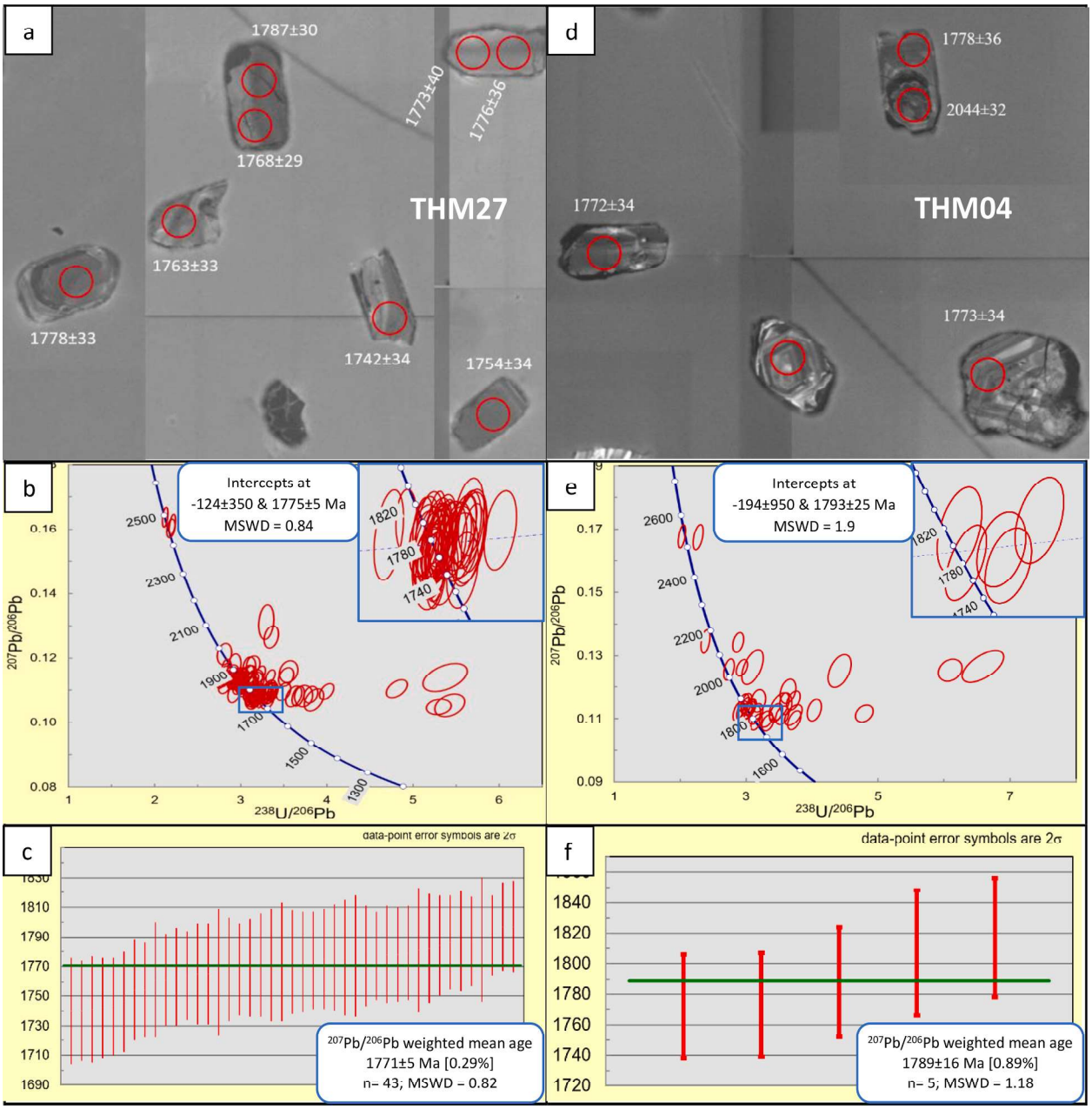


Fig. 14. Cathodoluminescence images for zircon grains from the youngest age group. Concordia diagrams for all analyses and concordant grains in the youngest age group (inset), and weighted mean age diagrams for the youngest zircon group for samples THM27 (a, b, and c, respectively) and THM04 (d, e, and f, respectively).

is interpreted as a sedimentary horizon and the zircons to be detrital.

6. Discussion

The presence of coarse gold grains as inclusions in peak-metamorphic hornblende and pyroxene suggests that at least some of the gold at Tick Hill was present prior to or during D_1 events (Laing, 1993; Choy, 1994; Le et al., 2021). However, on outcrop-scale the bulk of the gold is associated with syn-D_3 alteration assemblages and D_3 fracture zones. This indicates that most of the gold was either emplaced during D_3 events, or redistributed from an earlier gold deposit when large volumes of acidic, saline, oxidizing, aqueous fluids with the capacity to carry metals moved through much of the rock pile (Oliver et al., 1991; Laing, 1993; Tedman-Jones, 2001; Williams et al., 2005; Groves et al., 2010). Both early-gold and late-gold models have been pursued at some stage during the exploration history of Tick Hill and in either case intrusive activity was invoked as an underlying mechanism. Based on comparisons with the geology in the MKD, north of Tick Hill, the early D_1 events were assumed to have occurred within the Corella Formation around 1740 Ma, accompanied by the intrusion of Wonga and Burstall Suites (Blake et al., 1982; Wyborn, 1997). D_2 folding and $D_{3\text{-}4}$ faulting with gold mineralization was linked to Isan events between 1600 and 1500 Ma (e.g., Laing, 1993; Choy, 1994; Forrestal et al., 1998; Tedman-Jones, 2001). Whilst seemingly consistent with deformation and mineralization histories for IOCG deposits elsewhere in the Eastern Fold Belt (e.g., Williams et al., 2005), these interpretations are not consistent with the age data presented here.

The U-Pb zircon ages presented for igneous and quartzite units near the Tick Hill deposit, provide evidence for three distinct episodes of magmatic and/or metamorphic activity between 1855 Ma and 1520 Ma. These episodes are: (1) the emplacement of pre-D_1 granitic rocks at 1855–1850 Ma; (2) the emplacement of granite at 1790–1770 Ma

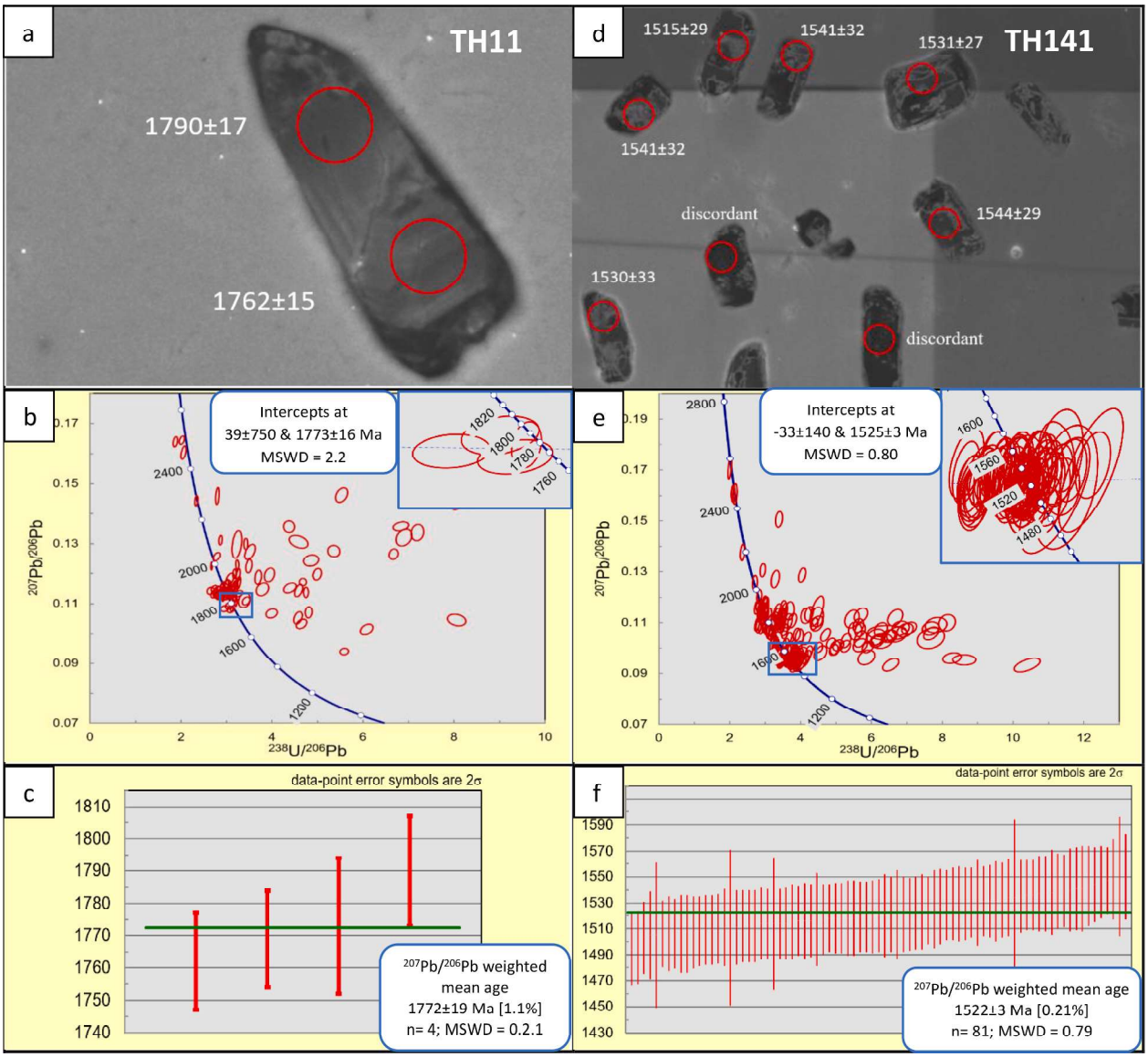


Fig. 15. Cathodoluminescence images for zircon grains from the youngest age group; concordia diagrams for all analyses and concordant grains in the youngest age group (inset); and weighted mean age diagrams for the youngest zircon group for samples TH11 (a, b, and c, respectively) and TH141 (d, e, and f, respectively).

concomitant with D_1 shearing and D_2 upright folding; and (3) 1525–1520 Ma, syn-D_3 pegmatite emplacement and related hydrothermal activity. Inheritance in many of the zircon populations suggests that older basement was present throughout much of the area, and there is a general lack of zircons with ages between 1740 and 1720 Ma, although a few appear in some of the younger pegmatite samples.

6.1. *The age of early igneous activity and deformation in the Tick Hill area*

Samples OTG and THG2 from granodiorite gneiss west of Tick Hill, have ages of 1857 ± 5 Ma and 1850 ± 6 Ma respectively, which are comparable to the age of the Kalkadoon Granodiorite that intruded the Leichhardt Volcanics (Wyborn and Page, 1983; Withnall and Hutton, 2013). Sample OTG was originally mapped as part of the Kalkadoon Supersuite (Blake et al., 1982) intruding the Plum Mountain Gneiss dated at 1863 Ma (Carson et al., 2011), which is consistent with our obtained age. Sample THG2 was collected from an outcrop originally mapped as part of the Wonga age (i.e., 1740 Ma) Tick Hill Complex (Blake et al., 1982; Wyborn, 1997). It was subsequently re-mapped as a small inlier of Burstall Suite (i.e., 1740 Ma), Saint Mungo Granite, within the Tick Hill Complex (Rutherford, 2000). Both the Tick Hill Complex and Saint Mungo Granite, based on historical data, were interpreted to intrude the Corella Formation, and rafts of Corella Formation gneiss occur within them (Wyborn, 1997; Rutherford, 1999; Rutherford, 2000). The new age data and geochemistry for THG2 indicate that the rock compares with the One Tree Granite, and that the unit is part of the Kalkadoon basement gneiss. The local outcrop of Kalkadoon basement surrounded by younger rocks (i.e. Tick Hill Complex, Fig. 3.1a) could be the remnant basement in the Tick Hill area or a block of basement rocks trapped into the intrusion of Tick Hill Complex. The mixing texture of metasediment and granitic gneiss within the outcrop (Fig. 3.1a) backups the later. The aeromagnetic signature of the unit from which sample THG2 was taken and its surrounding rocks (i.e. the large Tick Hill Granite body where sample THG4 were taken) is homogenous and similar to Kalkadoon basement gneiss further west. This suggests that (1) the Kalkadoon basement extends further east and locally occurs east of the mapped Argylla Formation (Blake et al., 1982) and (2) the large unit of Tick Hill granite mapped west of Tick Hill (Fig. 3a; Blake et al., 1982; Wyborn, 1997) possibly consists a large gneissic Kalkadoon basement.

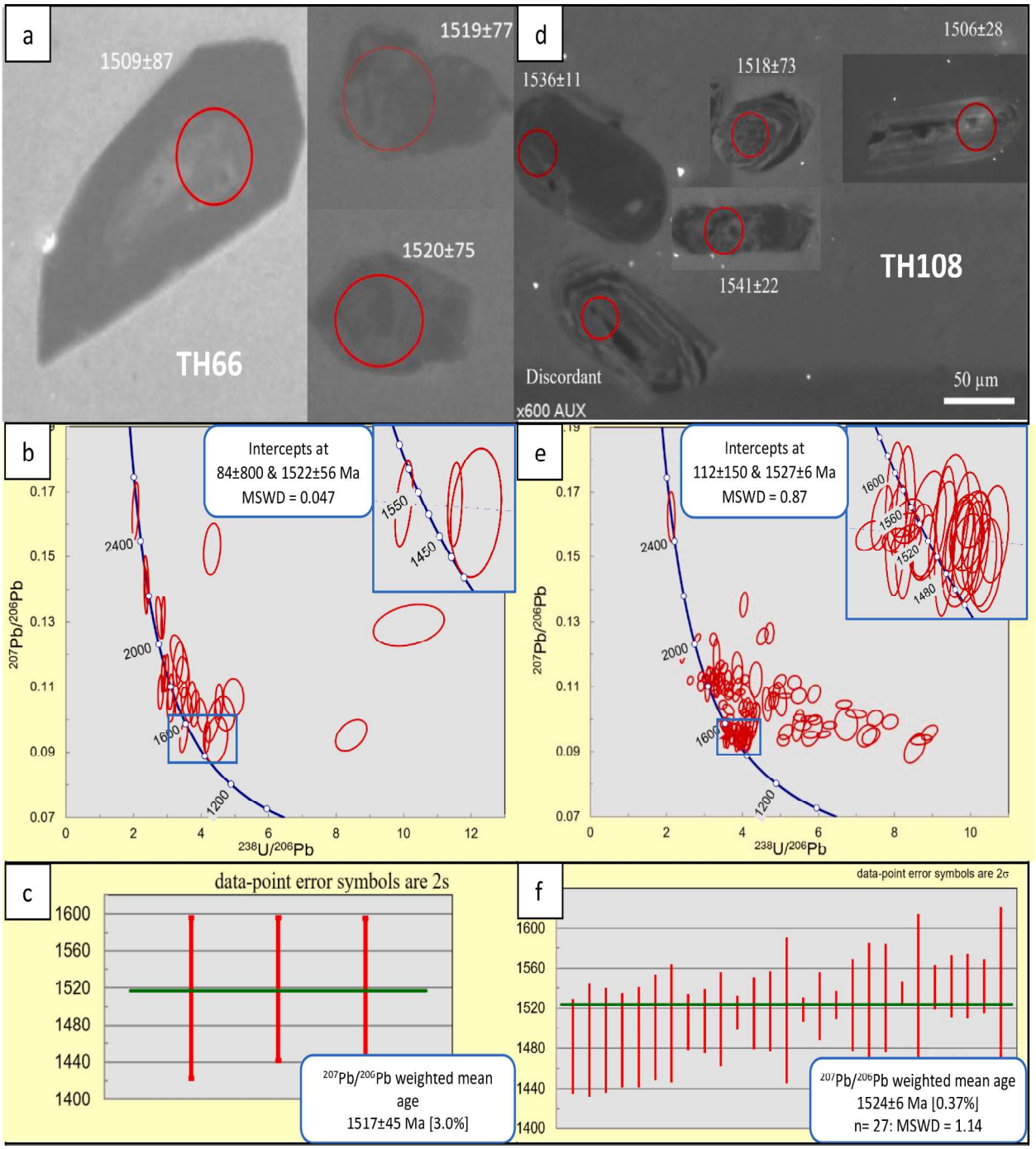


Fig. 16. Cathodoluminescence images for zircon grains from the youngest age group; concordia diagrams for all analyses and concordant grains in the youngest age group (inset), and weighted mean age diagrams for the youngest zircon group for samples TH66 (a, b, and c, respectively) and TH108 (d, e, and f, respectively).

Sample SMG of Saint Mungo Granite was originally mapped as part of the 1740 Ma Burstall Suite emplaced immediately west of the Argylla Formation (Blake et al., 1982; Wyborn, 1997). The new age (1790 ± 7 Ma) is well constrained and corresponds with the age of opening of the Leichhardt Superbasin in the Western Fold Belt (e.g., Foster and Austin, 2008; Withnall and Hutton, 2013), and particularly with the Big Toby-Yeldham-Bottletree igneous event (Carson et al., 2011; Withnall and Hutton, 2013). Geochemically and texturally, the sample is similar to THG1 (Figs. 7and 8), which yields a well-constrained age of 1777 ± 3 Ma and the two granites are probably related. THG1 was mapped as part of the Tick Hill Complex, but it occurs as a dyke intruding the remnant Kalkadoon Supersuit (i.e. sample THG2). It is texturally and chemically distinct from the leucogranites of the Tick Hill Complex that occur to the east (i.e., samples THG3, THG4, THM04, THM27, Figs. 7 and 8), and it is better described as part of the Saint Mungo Granite, to which it is geochemically similar. Both the SMG and THG1 samples have a well-developed gneissic layering, which is a composite $S_{1\text{-}2}$ foliation. The units were probably emplaced at some stage during D_1 and provide an age estimate for the earlier stages of this deformation event.

The four leucocratic granite samples (THG3, THG4, THM04, THM27) belonging to the Tick Hill Complex (Blake et al., 1982, Wyborn, 1997) are geochemically similar (Figs. 7 and 8). Their Si-rich nature and depletion in Ca, Mg, Ti, Zr and total REE, as well as the flat REE patterns with weak positive Eu anomalies are similar to the chemistry described

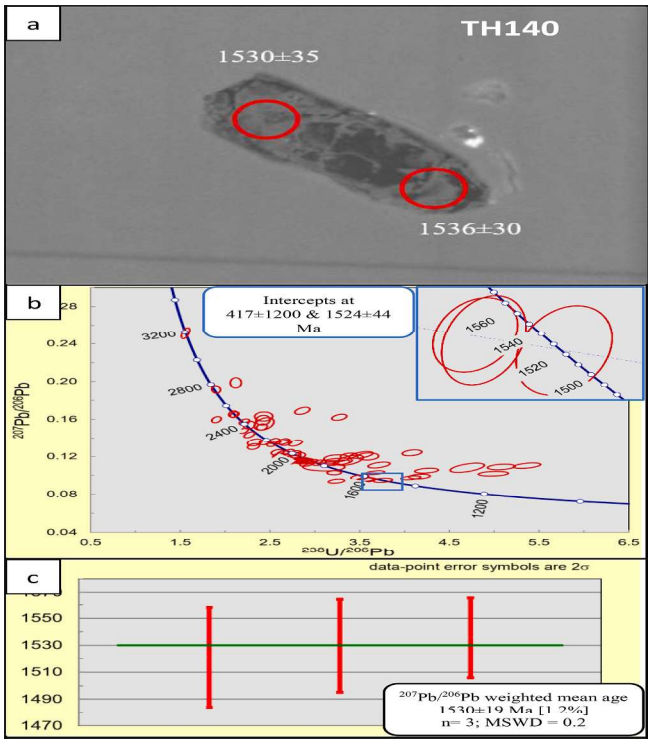


Fig. 17. Cathodoluminescence image for a representative zircon grain from the youngest age group, concordia diagram for all analyses and concordant grains in the youngest age group (inset), and weighted mean age diagrams for the youngest zircon group for sample TH140 (a, b, and c, respectively).

for low-temperature migmatites in which accessory phases were not fully resorbed in the melt (e.g., Solar and Brown, 2001; Bhadra et al., 2007; Sanislav et al., 2018). The leucogranites are interpreted as migmatitic segregations that were probably derived from the surrounding meta-pelite through partial melting. The close geochemical similarity between the leucogranites outside the pit (i.e., samples THG3 and THG4), which are of unambiguous granitic origin, and the heavily altered and mineralized quartzo-feldspathic mylonite (i.e., samples THM04, THM27) hosting the ore body, confirms that the latter originated as intrusions and not as immature sediments or laminated epithermal sinter deposits as has been proposed (e.g., England, 1993; England, 1995). The leucogranites from which the samples were taken vary texturally from strongly mylonitic (samples THM04, THM27) to almost undeformed with well-preserved graphic textures in which granite bodies appear to cross-cut the $S_{1\text{-}2}$ foliation and D_2 folds (e.g., THG4; Blake et al., 1982). The leucogranite pockets also display strong strain gradients with individual intrusive bodies characterized by mylonitic rims surrounding weakly deformed cores with characteristic coarse-grained graphic to pegmatoidal textures (sample THG3), whilst the fabric external to the granite bodies is mylonitic throughout. The field relationships, therefore, indicate that the Tick Hill granites intruded syn-tectonically during D_1 through to late-D_2 and their relatively uniform age of 1790–1770 Ma provides an upper age limit of $D_{1\text{-}2}$ deformation and metamorphism in the area. These relationships are confirmed by the 1773 ± 7 Ma age of the late tectonic (i.e., late-D_2) monzonite dyke (MG), which largely cuts the composite $S_{1\text{-}2}$ fabric and associated folding. The monzonite has a geochemical signature that is distinct from all other intrusions including the Monument Syenite (Figs. 7 and 8), and probably represents a separate late-tectonic intrusive phase.

In summary, it appears that most of the ductile deformation and igneous activity in the Tick Hill area occurred before 1770 Ma and involved two clear events, one around 1855–1850 Ma that can be linked to formation of the Leichhardt Volcanics at the end of the Barramundi Orogeny, and one around 1790–1770 Ma that can be linked to early Wonga events and regional deposition of Argylla volcanics during opening of the Leichhardt Basin (Page, 1978; Foster and Austin, 2008; Neumann et al., 2009; Carson et al., 2011; Magee et al., 2012; Withnall and Hutton, 2013; Kositcin et al., 2019). We have found no clear evidence for 1740 events, and the age of the syn-$D_{1\text{-}2}$ intrusions into the volcano-sedimentary sequence around Tick Hill clearly indicates that these sediments cannot be part of the Corella Formation. The remnant Kalkadoon basement gneiss units locally cropout further east than previously mapped (Blake et al., 1982, Wyborn, 1997), and appear to underlie the south MKD.

6.2. *The age of the sedimentary sequence in the Tick Hill area*

The sediments hosting the Tick Hill deposit were mapped as Corella Formation (Blake et al., 1982) and were, therefore, assumed to be 1740–1760 Ma (e.g., Tedman-Jones, 2001; Wyborn, 1997), despite an alternative interpretation in which the Corella Formation south of the Plum Mountain Fault Zone was correleated with >1860 Ma Plum Mountain Gneiss (Blake, 1980). The age of the Tick Hill granites and Saint Mungo Granite that intrude the sediments indicates that they must be older than at least ca. 1790 Ma, and, therefore, cannot be part of the Corella Formation. The two quartzitite samples were collected to constrain a maximum depositional age for the sediments, but the results are equivocal. The hanging wall quartzite yields a youngest age grouping with a weighted mean age of 1781 ± 6 Ma, but the ages were derived from mostly long-prismatic, zoned zircons that do not resemble detrital grains. In contrast, the footwall quartzite yields a youngest age population of 1841 ± 15 Ma, which does include zircon grains with a sedimentary appearance. This discrepency in ages suggests that the two parallel ridges are not related to one another and represent different units, and can be interpreted in several ways. If the youngest age population in each quartzite unit is interpreted as a sedimentary detrital population than the sediments must be younger than ca. 1781 Ma and could be the equivalent of the Ballara Quartzite (e.g., Page and Sun, 1998; Neumann et al., 2006). In this case they would have been deposited around the same time as deformation and metamorphism of the sediments invoking a very active tectinic regime for the paleo-basinal sequence. It also means that the data does not fit the intrusive relationships observed west of the pit (i.e. the problem of ca. 1790 Ma Saint Mungo Granites intruded into the ca. 1781 Ma sequence as being mapped in Rutherford, 1999; Rutherford, 2000). This suggests that different aged volcano-sedimentary rocks were infolded with each other along the D_1 high strain zone.

However, the quartzite ridges do not preserve unambiguous sedimentary features, and they were mapped by exploration teams in the 1990s as silicified shear zones, citing their disconinuous transgressive nature, diffuse boundaries, ghost gneiss fabrics and associated veining and fracturing (e.g., Laing 1993). The sample dated for the hanging wall quartzite, contains ~10% feldspar and acessory tourmaline that are alined in S_1, and were overprinted and largely replaced by quartz, with subsequent annealing and grain growth resulting in a coarse-grained massive texture. The sample displays similarities with heavily silicified quartz-feldspar mylonite in the same way that other samples collected from the same quartzite display similarities with silicified biotite schist or silicified calc-silicate (Wyborn, 1997). If the hanging wall quartzite sample is silicified leucogranite, then the zircons it contains will preserve prismatic igneous forms, and the minimum age (as well as older inherited ages) will be similar to other leucogranites; which is consistent with our observations (e.g., samples THM27 and TH13 have near-identical zircon populations). The footwall quartzite in contrast does not resemble silicified older lithologies, but looks more like a primary bedded sedimentary unit, and it preserves a different age population with a minimum age grouping of 1841 ± 15 Ma obtained from grains that inlude rounded grains (Appendix 4). The hanging wall quartzite also contains a major zircon grouping around 1841 ± 15 Ma and both

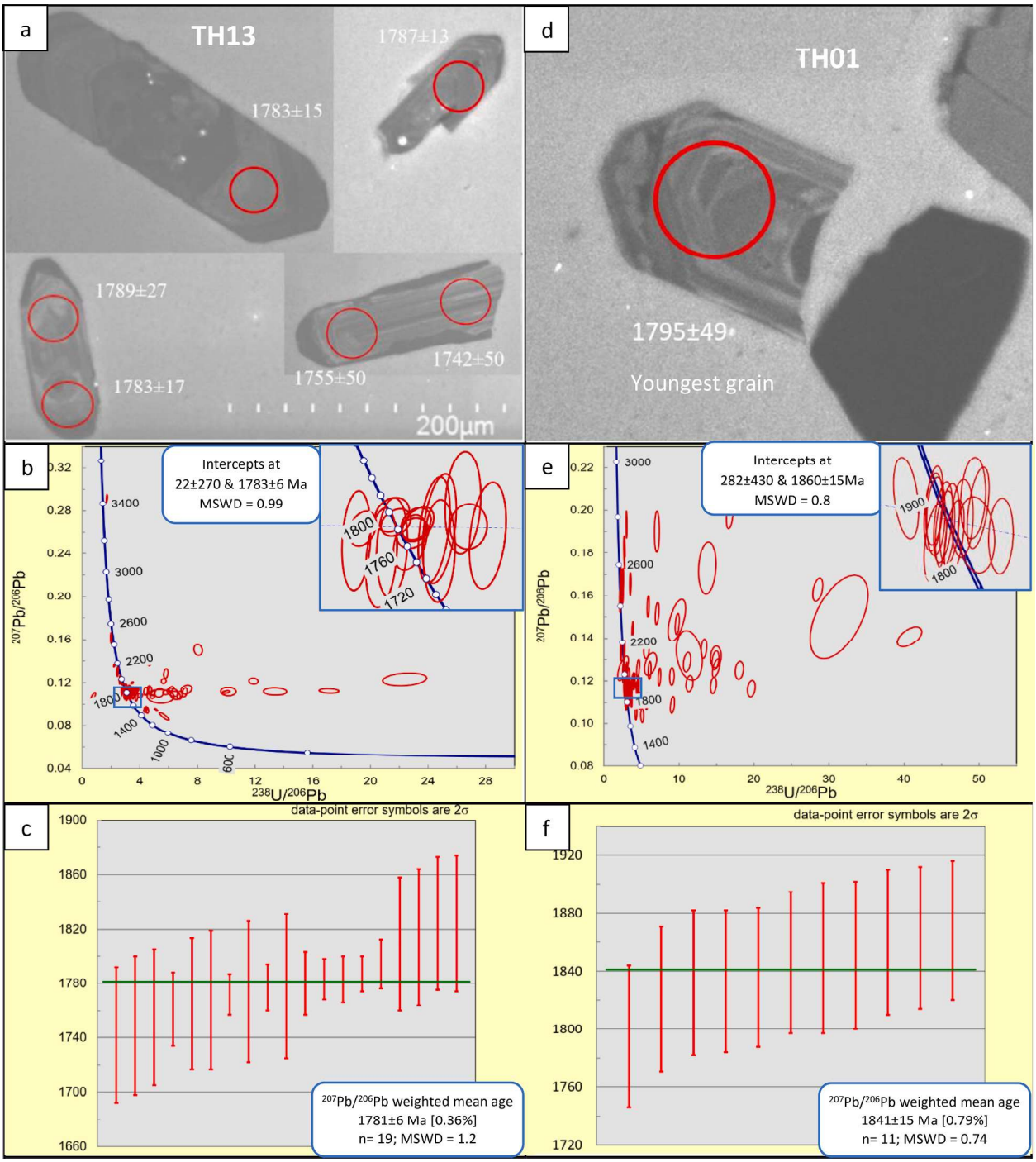


Fig. 18. Cathodoluminescence images for zircon grains from the youngest age group, concordia diagrams for all analyses and concordant grains in the youngest age group (inset), and weighted mean age diagrams for the youngest zircon group for samples TH13 (a, b, and c, respectively) and TH01 (d, e, and f, respectively).

samples contain significant numbers of pre-Barramundi grains. Considering this as well as the fact that the 1790 Ma Saint Mungo Granite described as intruding the Corella Formation (Blake et al., 1982), there is a strong possibility that the sedimentary sequence that hosts Tick Hill was formed sometime at 1841–1790 Ma and the equivalent of the "Old Corella Formation" as originally suggested by Blake (1980) and argued in Blake et al (1982).

6.3. *The timing of gold mineralization in the Tick Hill area*

The presence of coarse gold grains as inclusions in green hornblende and clinopyroxene in calc-silicate gneiss (Le et al., 2021) indicates that the metasedimentary rocks contained gold during D_1. It suggests that the gold was introduced before or during D_1 events at 1790–1770 Ma. Therefore, the age for this early gold stage is poorly constrained to sometime between 1855 Ma and 1770 Ma.

The main phase during which gold was either introduced or remobilized occurred during D_3 normal faulting and the associated fluid flux. The fluid flux resulted in the emplacement of en echelon arrays of pegmatite and quartz veins along the D_3 shear zones as well the formation of metasomatic, quartzo-feldspatic overgrowths replacing the earlier gneissic layering along the margins of some D_3 faults (Fig. 5d). Four of the five syn-D_3 pegmatite samples that were dated contain hydrothermal and metamict zircons with ages of around 1525–1520 Ma.

Whilst some of these pegmatites contain a wide range of discordant zircon grains with few concordant ages, TH141 and TH108 returned robust ages of 1522 ± 3 Ma and 1524 ± 6 Ma respectively, in which hydrothermal zircon interpreted to reflect metasomatic events and metamict zircon interpreted to reflect magmatic events yielded near-identical results. This suggests that the different types of zircon formed during a single episode when pegmatite veins were emplaced and hydrothermal fluids passed through, to alter the pegmatites and deposit gold. The ages are also consistent with poorly-constrained titanite age of 1517 ± 10 Ma, which was linked to mineralization (Tedman-Jones, 2001). The fifth pegmatite vein (TH11) only contained older concordant grains with an age of 1772 ± 19 Ma. The weakly deformed texture of this pegmatite sample likely resulted from the D_3 deformation event, and the youngest zircon cluster of 1772 ± 19 Ma possibly represent an inherited age.

Metamorphic-hydrothermal events dated at 1500–1530 Ma have been recorded by metamorphic titanite or zircon from a number of localities in the MKD to the north of Tick Hill (Page and Sun, 1998; Davis et al., 2001; Kositcin et al., 2019). Similar events are also widespread in the Easten Fold Belt where they have been linked to the emplacement of the Williams and Naraku granite suites and a regional fluid flux of highy oxidizing, saline fluids resulting in regional albite-hematite-scapolite alteration and IOCG type mineralization (e.g., Oliver, 1995; Oliver et al., 2004; Williams et al., 2005; Withnall and Hutton, 2013). In the Tick Hill area, there are no major 1525–1520 Ma intrusions associated with the observed albite-hematite alteration, but late pegmatites are common (Blake et al., 1982; Coughlin, 1993). The positive Eu anomalies recorded in the pegmatite samples (Fig. 7f) could reflect the elevated content of feldspar in pegmatite (Rollinson, 1993).

7. Conclusions

Dating of intrusive rocks and quartzite units around Tick Hill has placed constraints on the age of the main stratigraphic units in the area and has shown that existing stratigraphic and structural interpretations must be reviewed. Major igneous events occurred around 1855–1850 Ma and 1790–1770 Ma, and were followed by later hydrothermal events with pegmatite emplacement around 1525–1520 Ma. The age of the sediments in the Tick Hill area intruded by 1790–1770 Ma intrusions is therefore >1790 Ma. This is consistent with the maximum age (ca. 1841 ± 15 Ma) for a provenance zircon sample from footwall quartzite. Hanging wall quartzite contains a younger zircon population (ca. 1781 Ma) suggesting a younger age for the sediments, but this population can be interpreted differently if one considers that the quartzite is possibly metasomatic in origin, with silicification overprinting an intrusive quartzo-feldspathic gneiss. Major deformation and metamorphic events occurred between 1790 and 1770 Ma with the development of an upper amphibolite facies, mylonitic fabric (D_1), migmatization, and later upright folding (D_2). There probably were earlier fabrics associated with ca. 1850 Ma events, considering the composite nature of S_1, but these were transposed in the high strain D_1 fabric. Later extensional faulting and hydrothermal alteration events took place at 1525–1520 Ma during D_3, followed by younger strike-slip faulting (D_4) with an unconstrained age. The presence of hydrothermal zircon grains in pegmatite with a variety of ages between 1650 and 1520 Ma, suggests that Isan events affected the area to some degree, but these events did not leave a clear deformation imprint.

Formation of the gold ore body advanced in at least two stages: an early stage after deposition of the sediments and before or during D_1 events (1790–1770 Ma); and a late stage concomitant with D_3 events at 1525–1520 Ma. The later gold event left the clearest footprint and determined the current distribution pattern of the gold. The geochemistry of the quartzo-feldspathic mylonites that host the main ore zones, is consistent with that of $D_{1\text{-}2}$ leucogranite migmatitic origin. Therefore the quartzo-feldspathic mylonites were probably emplaced as leucogranite sills during D_1 and D_2.

One of the major outcomes of this study is that the "Old Corella Formation" or a new unnamed formation aged sometime between 1841 Ma and 1790 Ma appears to host the Tick Hill deposit, and the similar host rocks in the region is, therefore, prospective for gold mineralization (with anomalous Bi; Le et al., 2021).

CRediT authorship contribution statement

Truong X. Le: Conceptualization, Data curation, Formal analysis, Investigation, Methodology, Visualization, Writing – original draft. **Paul H.G.M. Dirks:** Supervision, Project administration, Writing - review & editing, Investigation, Validation. **Ioan V. Sanislav:** Supervision, Investigation, Validation. **Jan M. Huizenga:** Supervision, Validation. **Helen A. Cocker:** Methodology. **Grace N. Manestar:** Methodology, Formal analysis.

Declaration of Competing Interest

The authors declare that they have no known competing financial interests or personal relationships that could have appeared to influence the work reported in this paper.

Acknowledgements

We would like to thank the Geological Survey of Queensland (GSQ), the Economic Geology Research Centre (EGRU) at James Cook University (Townsville) and Rick Valenta who provided support to conduct this study. We would like to thank Peter Rea, Alex Brown and other personnel from Glencore, Mount Isa Mines and Paul Tan, Brett Davis and Rob Watkins in Carnaby Resources for providing logistical support for fieldwork, and access to drill core and data sets. Our thanks to Nick Oliver for donating Tick Hill samples for this study. We acknowledge Yi Hu and Huang Huiqing from JCU for help with LA-ICP-MS zircon dating. Our thanks to Kaylene Camuti for help with editing early versions of the manuscript. We would like to thank the reviewers for their appreciated comments. Funding for this study was provided by the Queensland Department of Natural Resources, Mines and Energy.

Appendix A. Supplementary data

Supplementary data to this article can be found online at https://doi.org/10.1016/j.precamres.2021.106422.

References

Abu Sharib, A.S.A.A., Sanislav, I.V., 2013. Polymetamorphism accompanied switching in horizontal shortening during Isan Orogeny: Example from the Eastern Fold Belt, Mount Isa Inlier, Australia. Tectonophysics 587, 146–167.

Alagna, K.E., Petrelli, M., Perugini, D., Poli, G., 2008. Micro-analytical zircon and monazite U-Pb isotope dating by laser ablation-inductively coupled plasma-quadrupole mass spectrometry. Geostand. Geoanal. Res. 32 (1), 103–120.

Betts, P.G., Giles, D., Mark, G., Lister, G.S., Goleby, B.R., Aillères, L., 2006. Synthesis of the Proterozoic evolution of the Mt Isa Inlier. Aust. J. Earth Sci. 53 (1), 187–211.

Bhadra, S., Das, S., Bhattacharya, A., 2007. Shear zone-hosted migmatites (Eastern India): the role of dynamic melting in the generation of REE-depleted felsic melts, and implications for disequilibrium melting. J. Petrol. 48 (3), 435–457.

Blake, D.H., 1980. The early geological history of the Proterozoic Mt Isa Inlier, northwestern Queensland: an alternative interpretation. BMR J. Aust. Geol. Geophys. 5, 243–256.

Blake, D.H., Bultitude, R.J., Donchak, P.J.T., 1982. Dajarra, Queensland 1:100000 geological map commentary. BMR Geol. Geophys. 225, 83 pp.

Blake, D.H., Bultitude, R.J., Donchak, P.J.T., 1984. Geology of the Duchess-Urandangi region, Mt Isa Inlier, Queensland. BMR Geol. Geophys. Aust. Bull. 219, 1–91.

Blake, D.H., 1987. Geology of the Mt Isa inlier and environs, Queensland and Northern Territory. BMR Geol. Geophys. Aust. Bull. 225, 1–83.

Blake, D., Steward, A., 1992. Stratigraphic and tectonic framework, Mt Isa. AGSO Bull. 243, 1–11.

Bodorkos, S., Purdy, D.J., Bultitude, R.J., Lewis, C.J., Jones, S.L., Brown, D.D., Hoy, D., 2020. Summary of Results. Joint GSQ-GA Geochronology Project: Mary Kathleen Domain and Environs, Mt Isa Inlier, 2018-2020. Queensland Geological Record 2020/04.

Carson, C., Hutton, L., Withnall, I., Perkins, W., 2009. Summary of results: Joint GSQ-GA NGA geochronology project, Mt Isa region, 2007–2008. Queensland Geological Record 2008/05.
Carson, C., Hutton, L., Withnall, I., Perkins, W., Donchak, P., Parsons, A., Blake, P., Sweet, I., Neumann, N., Lambeck, A., 2011. Summary of results: Joint GSQ-GA geochronology project, Mt Isa region, 2009-2010. Queensland Geological Record 2011/03.
Choy, D.K.W., 1994. The geology, structure, petrology, alteration and mineralization of Tick Hill, North-West Queensland. Master Thesis. Monash University, p. 220 pp..
Corfu, F., Hanchar, J.M., Hoskin, P.W., Kinny, P., 2003. Atlas of zircon textures. Rev. Miner. Geochem. 53 (1), 469–500.
Coughlin, T.J., 1993. Burke River; QLD; EPM 9083; Tick Hill Enclave 1:10000 Geological Mapping Programme. Internal MIMEX Report, Record No. 8548, Mt Isa exploration office.
Davis, B.K., Pollard, P.J., Lally, J.H., McNaughton, N.J., Blake, K., Williams, P.J., 2001. Deformation history of the Naraku Batholith, Mt Isa Inlier, Australia: implications for pluton ages and geometries from structural study of the Dipvale Granodiorite and Levian Granite. Aust. J. Earth Sci. 48 (1), 113–129.
Denaro, T.J., Randall, R.E., Smith, R.J., 2013. Chapter 10: Mineral and Energy Resources, in; Jell, P.A. (Eds): Geology of Queensland, Geological Survey of Queensland, Brisbane, pp 687-762.
England, R.N., 1993. Petrographic report for 35 samples from Tick Hill. Report to MIM Exploration Pty Ltd. ISAMISREP.018, Record No. 30874, Mt Isa exploration office.
England, R.N., 1995. The Tick Hill sedimentary exhalative gold deposit. Report to MIM Exploration Pty Ltd. ISAMISREP.023, Record No. 30881, Mt Isa exploration office.
Forrestal, P., Pearson, P., Coughlin, T., Schubert, C., 1998. In: Tick Hill Gold Deposit. Geology of the Mineral Deposits of Australia and Papua New Guinea. Australian Institute of Mining and Metallurgy, Carlton South, VIC, Monograph, pp. 699–706.
Foster, D.R., Austin, J.R., 2008. The 1800–1610Ma stratigraphic and magmatic history of the Eastern Succession, Mt Isa Inlier, and correlations with adjacent Paleoproterozoic terranes. Precambrian Res. 163 (1), 7–30.
Fricker, M.B., Kutscher, D., Aeschlimann, B., Frommer, J., Dietiker, R., Bettmer, Jörg, Günther, D., 2011. High spatial resolution trace element analysis by LA-ICP-MS using a novel ablation cell for multiple or large samples. Int. J. Mass Spectrom. 307 (1-3), 39–45.
Geoscience Australia, 2011. Geoscience Australia Geochron Delivery database. <http://www.ga.gov.au/geochron-sapub-web/>.
Groves, D.I., Bierlein, F.P., Meinert, L.D., Hitzman, M.W., 2010. Iron oxide copper-gold (IOCG) deposits through Earth history: implications for origin, lithospheric setting, and distinction from other epigenetic iron oxide deposits. Econ. Geol. 105 (3), 641–654.
Huston, D.L., Stevens, B., Southgate, P.N., Muhling, P., Wyborn, L., 2006. Australian Zn-Pb-Ag ore-forming systems: a review and analysis. Econ. Geol. 101 (6), 1117–1157.
Holcombe, R., Pearson, P., Oliver, N., 1991. Geometry of a middle Proterozoic extensional decollement in northeastern Australia. Tectonophysics 191 (3–4), 255–274.
Jackson, M.J., Scott, D.L., Rawlings, D.J., 2000. Stratigraphic framework for the Leichhardt and Calvert Superbasins: review and correlations of the pre-1700 Ma successions between Mt Isa and McArthur River. Aust. J. Earth Sci. 47 (3), 381–403.
Jackson, S.E., Pearson, N.J., Griffin, W.L., Belousova, E.A., 2004. The application of laser ablation-inductively coupled plasma-mass spectrometry to in situ U-Pb zircon geochronology. Chem. Geol. 211 (1-2), 47–69.
Kositcin, N., Bultitude, R.J., Purdy, D.J., 2019. Queensland Geological Record 2019/02. Summary of results. Joint GSQ-GA Geochronology Project: Mary Kathleen Domain, Mt Isa Inlier, 2018-2019. Queensland Geological Record 2019/02.
Kwelwa, S.D., Sanislav, I.V., Dirks, P.H.G.M., Blenkinsop, T., Kolling, S.L., 2018. ZirconU-Pb ages and Hf isotope data from the Kukuluma Terrain of the Geita Greenstone Belt, Tanzania Craton: implications for stratigraphy, crustal growth and timing of gold mineralization. J. Afr. Earth Sci. 139, 38–54.
Laing, W.P., 1993. Geology of the Tick Hill region, Mt Isa, with implications for exploration. Report to MIM Exploration Pty Ltd., ISAMISREP.017; Record No. 30870, Mt Isa exploration office.
Le, T.X., Dirks, P.H.G.M., Sanislav, I.V., Huizenga, J.M., Cocker, H., Manestar, G.N., 2021. Geological setting and mineralization characteristics of the Tick Hill Gold Deposit, Mt Isa Inlier, Queensland, Australia. Ore Geol. Rev. 137, 104288.
Ludwig, K.R., 2011. User's Manual for Isoplot 4.15: A Geochronological Toolkit for Microsoft Excel. Berkeley Geochronology Center, Berkeley, California, U.S.A.
MacCready, T., Goleby, B., Goncharov, A., Drummond, B., Lister, G., 1998. A framework of overprinting orogens based on interpretation of the Mt Isa deep seismic transect. Econ. Geol. 93 (8), 1422–1434.
Magee, C.W., Withnall, I.W., Hutton, L.J., Perkins, W.G., Donchak, P.J.T., Parsons, A., Blake, P.R., Sweet, I.P., Carson, C.J., 2012. Joint GSQ-GA geochronology project, Mount Isa Region, 2008-2009. Record 2012/07, Queensland Geological Survey, Brisbane.
McDonough, W.F., Sun, S.-s., 1995. The composition of the Earth. Chem. Geol. 120 (3-4), 223–253.
Middlemost, E.A.K., 1994. Naming materials in the magma/igneous rock system. Earth Sci. Rev. 37 (3-4), 215–224.
Neumann, N., Southgate, P., Gibson, G., McIntyre, A., 2006. New SHRIMP geochronology for the Western Fold Belt of the Mt Isa Inlier: developing a 1800–1650 Ma event framework. Aust. J. Earth Sci. 53 (6), 1023–1039.
Neumann, N.L., Fraser, G.L., 2007. Geochronological synthesis and time-space plots for Proterozoic Australia. Geoscience Australia Record 2007/06.
Neumann, N.L., Gibson, G.M., Southgate, P.N., 2009. New SHRIMP age constraints on the timing and duration of magmatism and sedimentation in the Mary Kathleen Fold Belt, Mt Isa Inlier, Australia. Aust. J. Earth Sci. 56 (7), 965–983.
Oliver, N.H.S., Holcombe, R.J., Hill, E.J., Pearson, P.J., 1991. Tectono-metamorphic evolution of the Mary Kathleen Fold Belt, northwest Queensland: a reflection of mantle plume processes? Aust. J. Earth Sci. 38 (4), 425–455.
Oliver, N.H.S., 1995. Hydrothermal history of the Mary Kathleen Fold Belt, Mt Isa Block, Queensland. Aust. J. Earth Sci. 42 (3), 267–279.
Oliver, N.H.S., Cleverley, J.S., Mark, G., Pollard, P.J., Fu, B., Marshall, L.J., Rubenach, M. J., Williams, P.J., Baker, T., 2004. Modeling the Role of sodic alteration in the genesis of iron oxide-copper-gold deposits, Eastern Mt Isa Block, Australia. Econ. Geol. 99 (6), 1145–1176.
O'dea, M.G., Lister, G., MacCready, T., Betts, P., Oliver, N., Pound, K., Huang, W., Valenta, R., 1997. Geodynamic evolution of the Proterozoic Mt Isa terrain. Geol. Soc., London, Spec. Publ. 121 (1), 99–122.
Paces, J.B., Miller Jr, J.D., 1993. Precise U-Pb ages of Duluth complex and related mafic intrusions, northeastern Minnesota: Geochronological insights to physical, petrogenetic, paleomagnetic, and tectonomagmatic processes associated with the 1.1 Ga midcontinent rift system. J. Geophys. Res.: Solid Earth 98 (B8), 13997–14013.
Page, R., 1978. Response of U-Pb Zircon and Rb-Sr total-rock and mineral systems to low-grade regional metamorphism in proterozoic igneous rocks, Mt Isa, Australia. J. Geol. Soc. Aust. 25 (3–4), 141–164.
Page, R., 1983. Chronology of magmatism, skarn formation, and uranium mineralization, Mary Kathleen, Queensland, Australia. Econ. Geol. 78 (5), 838–853.
Page, R.W., Sun, S-S., 1998. Aspects of geochronology and crustal evolution in the Eastern Fold Belt, Mt Isa Inlier. Aust. J. Earth Sci. 45 (3), 343–361.
Passchier, C., Williams, P., 1989. Proterozoic extensional deformation in the Mt Isa inlier, Queensland, Australia. Geol. Mag. 126 (1), 43–53.
Passchier, C., 1992. Geology of the Myubee area, Mt Isa Inlier, Queensland. Detailed studies of Mt Isa Inlier, pp. 199-208.
Paton, C., Hellstrom, J., Paul, B., Woodhead, J., Hergt, J., 2011. Iolite: Freeware for the visualisation and processing of mass spectrometric data. J. Anal. Atom. Spectrom. 26 (12), 2508–2518.
Pearson, P., Holcombe, R., Page, R., 1992. Synkinematic emplacement of the Middle Proterozoic Wonga Batholith into a mid-crustal extensional shear zone, Mt Isa Inlier, Queensland, Australia. In: Detailed Studies of the Mt Isa Inlier, pp. 289–328.
Perkins, C., Wyborn, L., 1998. Age of Cu-Au mineralization, Cloncurry district, eastern Mt Isa Inlier, Queensland, as determined by 40Ar/39Ar dating. Aust. J. Earth Sci. 45 (2), 233–246.
Pettke, T., 2008. Analytical protocols for element concentration and isotope ratio measurements in fluid inclusions by LA-(MC)-ICP-MS. Laser Ablation ICP-MS in the Earth Sciences: Current Practices and Outstanding Issues. Mineral. Assoc. Canada, Short Course Ser. 40, 189–218.
Richards, J.R., Cooper, J.A., Webb, A.W., 1963. Potassium-argon ages on micas from the Precambrian region of North-Western Queensland. J. Geol. Soc. Aust. 10 (2), 299–312.
Rollinson, H., 1993. In: Using Geochemical Data: Evaluation, Presentation, Interpretation. Longman Group UK Ltd, London, p. 352.
Rutherford, N.F., 1999. First annual joint venture report to 1st January 2000 for exploration permits for minerals 9083, 11012 & 11013, Burke River Region, Mt Isa-Cloncurry District, North West Queensland, Technical Report No: 1. <https://geoscience.data.qld.gov.au/report/cr030650>.
Rutherford, N.F., 2000. Second annual joint venture report to 1st January 2000 for exploration permits for minerals 9083, 11012 & 11013, Burke River Region, Mt Isa-Cloncurry District, North West Queensland, Technical Report No: 2. <https://geoscience.data.qld.gov.au/report/cr031587>.
Sanislav, I.V., Dirks, P.H.G.M., Blenkinsop, T., Kolling, S.L., 2018. 'The tectonic history of a crustal-scale shear zone in the Tanzania Craton from the Geita Greenstone Belt, NW Tanzania Craton. Precambrian Res. 310, 1–16.
Scott, D.L., Rawlings, D.J., Page, R.W., Tarlowski, C.Z., Idnurm, M., Jackson, M.J., Southgate, P.N., 2000. Basement framework and geodynamic evolution of the Palaeoproterozoic superbasins of north-central Australia: an integrated review of geochemical, geochronological and geophysical data. Aust. J. Earth Sci. 47 (3), 341–380.
Solar, G.S., Brown, M., 2001. Petrogenesis of migmatites in Maine, USA: possible source of peraluminous leucogranite in plutons? J. Petrol. 42 (4), 789–823.
Southgate, P., Neumann, N., Gibson, G., 2013. Depositional systems in the Mt Isa Inlier from 1800 Ma to 1640 Ma: Implications for Zn–Pb–Ag mineralization. Aust. J. Earth Sci. 60 (2), 157–173.
Spence, J., Sanislav, I., Dirks, P., 2021. 1750–1710 Ma deformation along the eastern margin of the North Australia Craton. Precambrian Res. 353, 106019.
Tedman-Jones, C., 2001. Tick Hill core relogging review. Internal report to MIM Exploration Pty Ltd. Misc.2001/010, Record No: 30764. Mt Isa exploration office.
Tucker, R.T., Roberts, E.M., Hu, Y., Kemp, A.I.S., Salisbury, S.W., 2013. Detrital zircon age constraints for the Winton Formation, Queensland: contextualizing Australia's Late Cretaceous dinosaur faunas. Gondwana Res. 24 (2), 767–779.
Wiedenbeck, M., Alle, P., Corfu, F., Griffin, W., Meier, M., Oberli, F., Quadt, A.V., Roddick, J., Spiegel, W., 1995. Three natural zircon standards for U-Th-Pb, Lu-Hf, trace element and REE analyses. Geostandards Newsl. 19 (1), 1–23.
Williams, P.J., Barton, M.D., Johnson, D.A., Fontboté, L., De Haller, A., Mark, G., Oliver, N.H., Marschik, R., 2005. Iron oxide copper-gold deposits: Geology, space-time distribution, and possible modes of origin. Econ. Geol. 371–405.
Withnall, I., Hutton, L., 2013. Chapter 2: North Australian Craton, in: Jell, P.A. (Eds): Geology of Queensland. Geology of QUeensland, Geological Survey of Queensland, Brisbane, pp. 23–112.
Withnall, I.W., 2019. Review of SHRIMP zircon ages for the Eastern Succession of the Mt Isa Province and magmatic events in its provenance. Queensland Minerals and Energy Review Series, Department of Natural Resources, Mines and Energy, Queensland.

Wyborn, L., Page, R., 1983. The Proterozoic Kalkadoon and Ewen batholiths, Mt Isa Inlier, Queensland-source, chemistry, age and metamorphism. BMR J. Geol. Geophys. 8 (1), 53–69.
Wyborn, L.A.I., 1997. Dajarra 1:100,000 digital geology, part of Mt Isa geological digital dataset. Geoscience Australia. <http://pid.geoscience.gov.au/dataset/ga/30923>.
Wyborn, L., Page, R., McCulloch, M., 1988. Petrology, geochronology and isotope geochemistry of the post-1820 Ma granites of the Mt Isa Inlier: mechanisms for the generation of Proterozoic anorogenic granites. Precambrian Res. 40, 509–541.